UNIVERSITY OF OKLAHOMA

GRADUATE COLLEGE

CHARACTERIZATION AND ASSESSMENT OF LONG-TERM POROSITY OF VARIOUS CEMENT FORMULATIONS UTILIZING NUCLEAR MAGNETIC RESONANCE (NMR) TECHNOLOGY

A THESIS

SUBMITTED TO THE GRADUATE FACULTY

in partial fulfillment of the requirements for the

Degree of

MASTER OF SCIENCE

By

ERETORU NIMI ROBERT

Norman, Oklahoma

2024

CHARACTERIZATION AND ASSESSMENT OF LONG-TERM POROSITY OF VARIOUS CEMENT FORMULATIONS UTILIZING NUCLEAR MAGNETIC RESONANCE (NMR) TECHNOLOGY

A THESIS APPROVED FOR THE

MEWBOURNE SCHOOL OF PETROLEUM AND GEOLOGICAL ENGINEERING

BY THE COMMITTEE CONSISTING OF

Dr. Catalin Teodoriu, Chair

Dr. Ahmed Ramadan

Dr. Deepak Devegowda

Acknowledgements

First and foremost, I would like to extend my deepest gratitude to my advisor, Dr. Catalin Teodoriu. His unwavering guidance, encouragement, and vast knowledge have been invaluable throughout my research journey. I am truly grateful for his patience, insight, and dedication, which have inspired me to challenge myself and to think critically in ways I had not anticipated.

I would also like to express my heartfelt thanks to my thesis committee members, Dr. Deepak Devegowda and Dr. Ahmed Ramadan. Their constructive feedback, thoughtful discussions, and expert advice have been instrumental in shaping this work and refining my ideas. Their support and guidance have been crucial throughout this work, and I deeply appreciate their time and effort.

I am incredibly thankful to my family for their constant love, support, and encouragement. Their faith in me has been my foundation and motivation, especially during challenging times. I am equally grateful to my friends who have been a steady source of laughter, understanding, and perspective. Their companionship has been essential in making this journey more balanced and enjoyable.

A special thanks to the University of Oklahoma and the Mewbourne School of Petroleum and Geological Engineering for providing the resources and environment necessary for my research.

Thank you all for being an essential part of this journey.

Eretoru Nimi Robert

Table of Contents

List of Figures

Tables

Equations

Abstract

The global increase in hydrocarbon demand has pushed the oil and gas industry to explore new reservoirs that were previously untapped due to the technological limitations associated with high-pressure and high-temperature conditions. This demand has concurrently driven the development of advanced well-construction materials capable of withstanding extreme environments while addressing the industry's environmental challenges. The production of conventional cement significantly contributes to carbon emissions, with approximately one kilogram of CO_2 released for each kilogram of cement produced, accounting for nearly 9% of global human-related emissions. This underlines the need for sustainable alternatives to reduce the carbon footprint of well cementing.

Geopolymers emerge as a viable solution, offering lower carbon emissions, high compressive strength, and superior resistance to chemical degradation, thereby aligning with the industry's sustainability objectives. This thesis explores the long-term NMR porosity behavior and pore size distribution of traditional cement (class G and class H) and geopolymers in well cementing, focusing on the effects of various additives, such as fly ash, silica flour, microcellulose, and microblock, across different curing conditions.

A comprehensive study was conducted using Nuclear Magnetic Resonance (NMR) technology to monitor NMR porosity evolution over extended curing periods: 146 days at room temperature and 35 days at 75°C. Results showed that at room temperature, the addition of fly ash led to substantial NMR porosity reduction demonstrating the most significant impact by enhancing the cement matrix's densification. The NMR analysis revealed a consistent shift toward smaller pores over time, indicative of ongoing hydration and pozzolanic reactions.

High-temperature curing demonstrated accelerated hydration and rapid porosity stabilization within the first 24 hours for fly ash-modified and geopolymer samples, which maintained stable NMR porosity levels throughout the testing period. The findings also suggests that increased fly ash content contributes to greater thermal stability and pore structure refinement under elevated temperatures. The study also established that prolonged curing time significantly influences NMR porosity reduction for all formulations in this work.

Overall, this research provides practical guidelines for optimizing cement formulations to enhance wellbore integrity across diverse environmental conditions, with an emphasis on sustainable and durable solutions for the oil and gas industry.

1 Introduction

1.1 Research Motivation

The world's population has experienced exponential growth over the past seven decades, more than tripling from 2.5 billion in 1950 to 8 billion in 2022. This rapid expansion is expected to continue, with projections indicating an additional 1.7 billion people by 2050 and 2.4 billion by 2100, reaching a potential peak of 10.4 billion in the mid-2080s.

Despite the uncertainty inherent in population projections, the United Nations anticipates the global population will reach 8.5 billion by 2030, 9.7 billion by 2050, and 10.4 billion by 2100 as seen in **Figure 1**. This unprecedented population growth poses significant challenges to global sustainability, resource management, and environmental stewardship, underscoring the need for innovative solutions and strategic planning (United Nations, 2024).

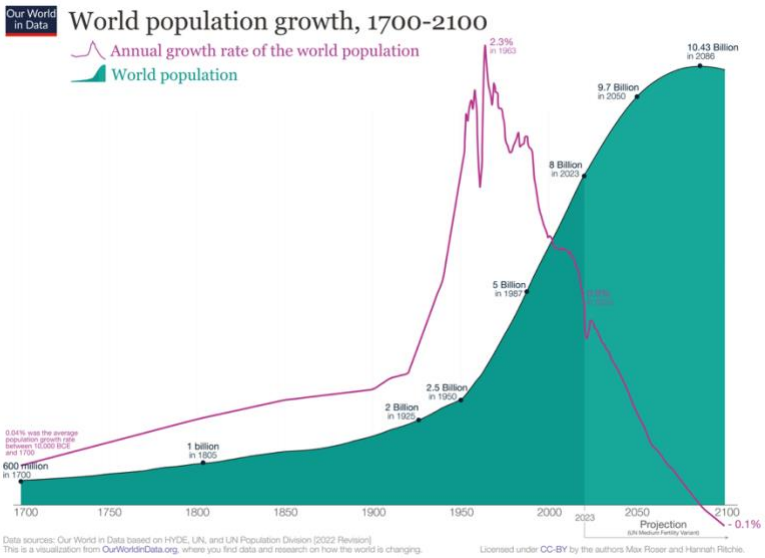

Figure 1: World population growth 1700–2100, 2022 projection (United Nations, 2024)

In 2023, declining electricity consumption in advanced economies limited the growth of global power demand, which increased by 2.2%, slightly below the 2.4% rise seen in 2022. However, global electricity demand is projected to grow at a quicker pace over the next three years, averaging 3.4% annually through 2026. This acceleration will be fueled by an improving economic outlook, leading to higher demand for electricity in both advanced and emerging markets (International Energy Agency, 2024). Global energy demand is set to rise by 15%, driven by population growth and expanding economies (ExxonMobil Global Outlook, 2024). Globally, electricity consumption is growing at a rate that surpasses population growth, resulting in a rise in the average electricity usage per person (per capita consumption) (U.S. Energy Information Administration, 2020) as depicted by **Figure 2**.

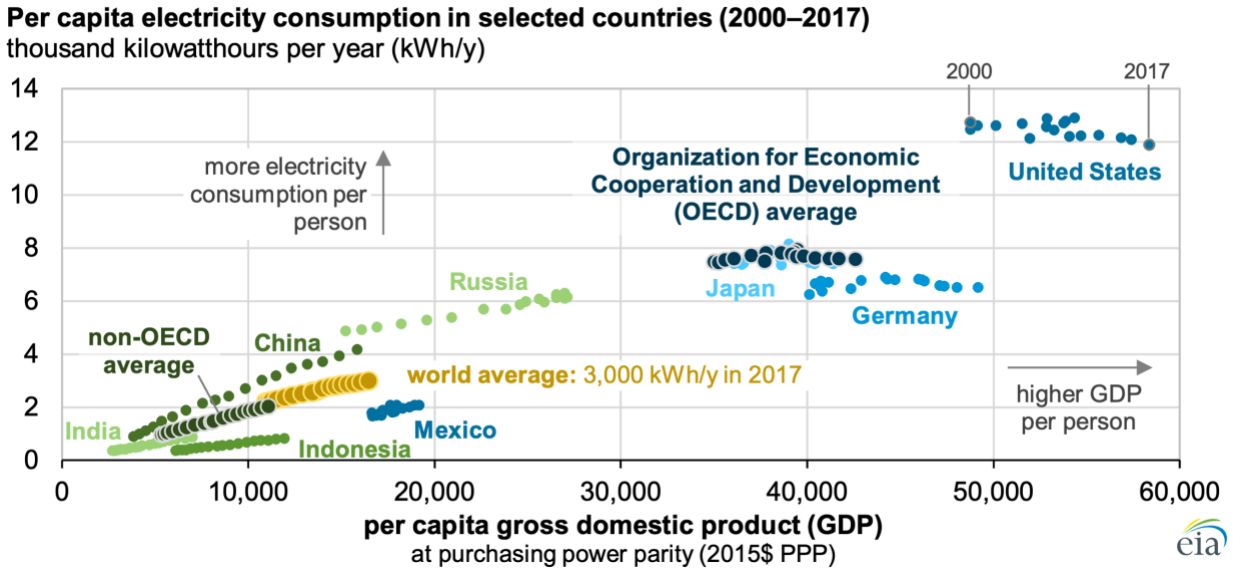

Figure 2: Per capita electricity consumption in selected countries (U.S. Energy Information Administration, 2020)

Historically, the oil and gas sector play a crucial role in driving the global economy and is one of the most significant industries worldwide, making substantial economic contributions. The energy

sector has a strong demand for labor, employing over 65 million people globally in 2019 (Investopedia, 2024).

Significant changes currently taking place are set to create a dramatically different global energy landscape by the end of this decade. The remarkable growth of clean energy technologies like solar, wind, electric vehicles, and heat pumps is transforming the way we power everything from factories and transportation to household appliances and heating systems (International Energy Agency, 2023).

Although progress has been made in expanding renewable energy sources (RES), the energy transition has been slower than anticipated due to key technologies still being immature, and lacking scalability, or cost-efficiency. These challenges, combined with increasing energy demand and limitations in renewable infrastructure, suggest that renewables alone will not be sufficient to meet global energy needs in the near term. As a result, fossil fuels—including oil, natural gas, and coal—are expected to continue playing a role in the global energy mix until 2050, covering 40% to 60% of demand, down from 78% in 2023, depending on the scenario (McKinsey & Company, 2024) as depicted by **Figure 3**.

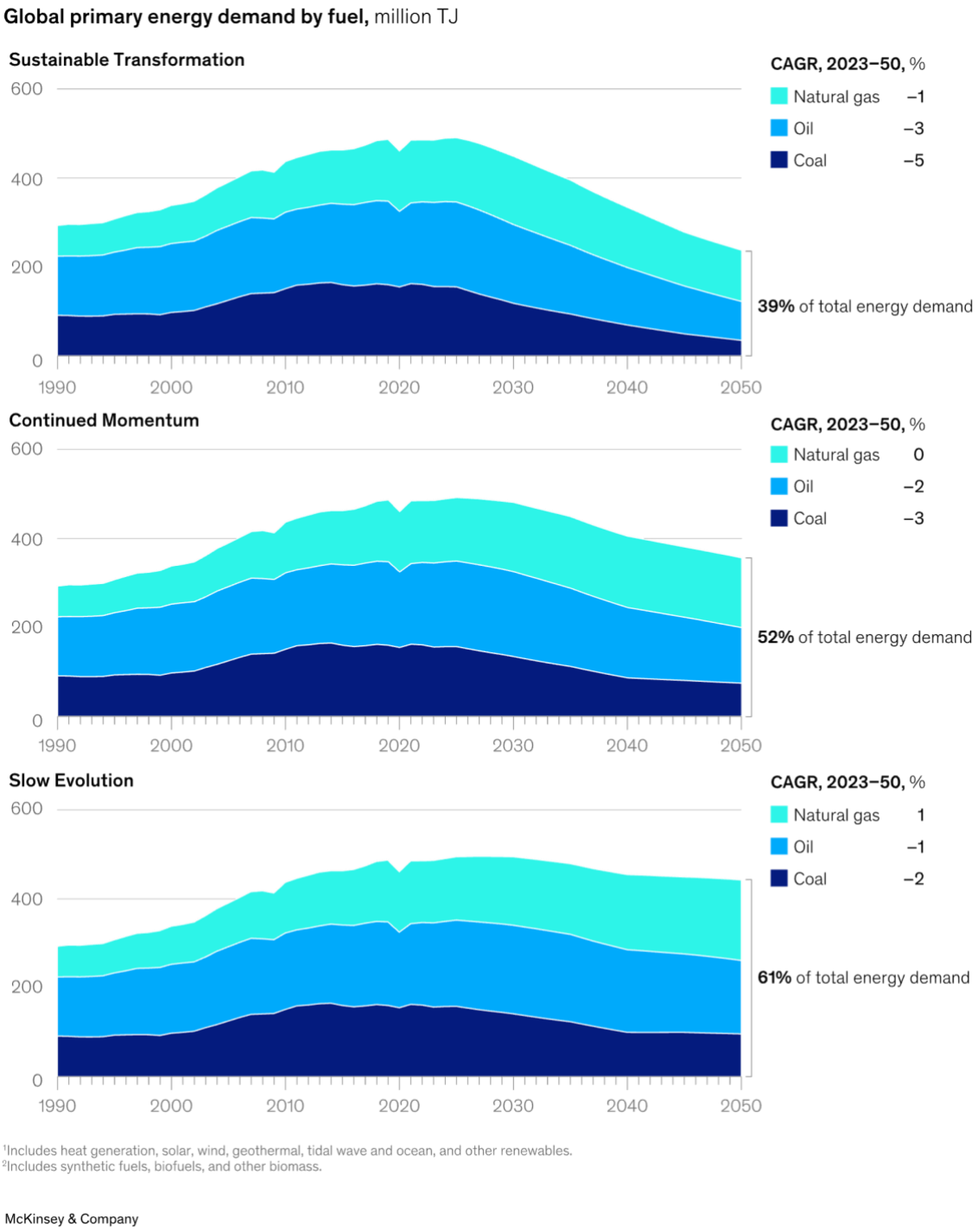

Figure 3: Fossil demand is projected to plateau before declining, but still accounts for 40 to 60 percent of energy demand in 2050 (McKinsey & Company, 2024)

Approximately 2 million oil and gas wells had been drilled worldwide as of 2022. Over the past decade, the number of newly drilled wells has varied considerably, with around 70,000 new wells added in 2022 alone, indicating the sector's resilience despite challenges such as volatile oil prices and the impacts of the COVID-19 pandemic. Major contributors to global onshore drilling activity include North America, China, and Russia, while significant offshore operations are present in areas like the Gulf of Mexico, Saudi Arabia, and the Norwegian Continental Shelf (S&P Global, 2022).

In 2022, the United States had roughly 913,000 operational oil and gas wells, marking a slight decline from the peak of over 1 million in 2014 (**Figure 4**). Despite the reduced number of wells, these continue to contribute significantly to U.S. energy production. Advances in technologies such as horizontal drilling have allowed the industry to sustain and even boost oil output, despite the drop in well count. This underscores the crucial role that oil and gas still play in fulfilling energy needs, even as the shift towards renewable energy gains momentum (U.S. Energy Information Administration, 2023).

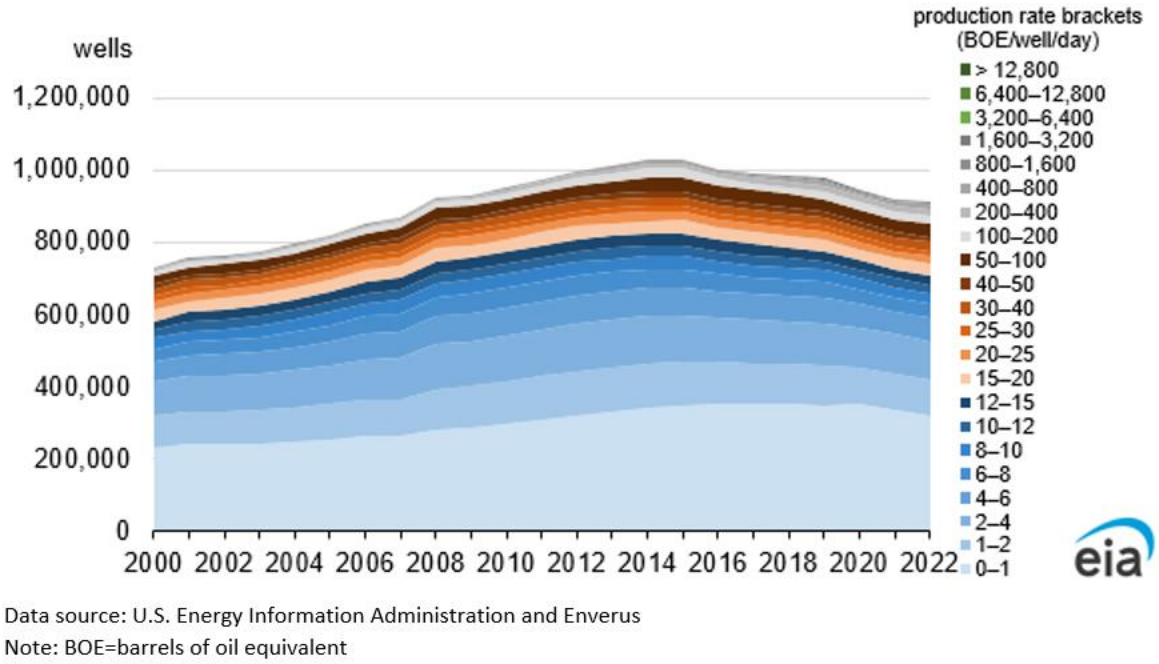

Figure 4: Total U.S. wells by production rate brackets (U.S. Energy Information Administration, 2023)

The oil and gas industry is facing increasing pressure to continuously innovate while maintaining stringent safety standards. As a result, substantial resources are now being invested in the development of advanced technologies aimed at enhancing well integrity, particularly in the area of well-cementing (Romero et al., 2022). Well-integrity is crucial to preventing environmental hazards, ensuring safety, and maintaining operational efficiency. Globally, about 30-45% of active wells face some kind of integrity issue, such as sustained annulus pressure or barrier failures, highlighting the need for continuous monitoring and maintenance throughout the well's life cycle (Yakoot et al., 2021). Well-cementing plays a pivotal role in maintaining wellbore integrity, acting as a critical barrier between the casing and the formation. This barrier not only provides mechanical support and zonal isolation but also helps prevent casing corrosion and ensures long-term well stability. The proper design and application of cement are essential in mitigating risks associated with well construction, such as de-bonding, micro-annuli, and compromised cement quality, which

could otherwise jeopardize the integrity of the entire well structure (Teodoriu et al., 2010). This focus reflects the industry's commitment to both technological advancement and safety in operations.

Ensuring well integrity is crucial in drilling operations, where cement serves as a primary sealant to prevent fluid migration between geological formations. The efficiency of cement in fulfilling this role largely depends on its porosity, which influences its permeability, mechanical strength, and resistance to chemical attack. As the industry explores deeper and more challenging environments, optimizing cement formulations to withstand high pressures, temperatures, and aggressive fluids becomes even more important. Incorporating additives into the base cement can modify its pore structure and improve its performance, making it vital to understand how these changes impact the cement's long-term properties.

Cement porosity is a critical factor in well integrity, as it directly affects the ability of the cement to serve as an effective barrier in the wellbore. An understanding of this important property and how incorporating different additives such as fly ash, silica flour, micro cellulose, and microblock to cement affects the behavior of the cement is cogent for not just the oil and gas industry but geothermal as well as cement is used in both completion and intervention processes.

1.2 Objectives

1.2.1 General objective

The overarching aim of this work is to characterize and evaluate the long-term NMR porosity of various cement formulations utilizing non-destructive testing. Typically, cement porosity measurement requires the samples to be dried, which can affect hydration and alter the results. Nuclear Magnetic Resonance (NMR) technology, however, is a technique that allows for the measurement of pore structure and fluid content in cement without altering the hydration process.

This approach provides accurate insights into the evolution of porosity over time, enabling the assessment of the cement's durability and performance under different curing conditions.

This objective was accomplished by curing and measuring the porosity under room temperature conditions for a period of 146 days (~5 months). Additionally, the porosity of selected samples was measured under high-temperature conditions for a period of 35 days.

1.2.2 Specific objectives

- Conduct a comprehensive literature review focused on well cementing and well integrity, along with an overview of cement porosity and additives materials in the oil and gas industry.
- Evaluate the impact of incorporating fly ash, silica flour, micro cellulose, and micro block on the long-term porosity of class G cement and incorporating fly ash in class H cement under room temperature conditions using Nuclear Magnetic Resonance (NMR) technology.
- Measure and analyze the porosity changes in various cement formulations over a period of 146 days (~5 months) under room temperature conditions.
- Measure and analyze the porosity changes in geopolymer over a period of 146 days (~5 months) cured under elevated temperature conditions
- Determine the effects of elevated temperatures on the porosity of selected cement samples over a period of 35 days.
- Evaluate and compare the porosity behavior of various cement formulations (with and without additives) to identify optimal compositions for wellbore integrity.
- Investigate how varying curing times impact the porosity of different cement formulations.
- Provide guidelines for selecting and applying optimal cement formulations based on the study's findings, considering factors such as wellbore conditions and temperature.

1.3 Scope of work

The scope of this work centers on the characterization and evaluation of the long-term porosity evolution in class G cement formulations with various additives, including fly ash (FA), microblock (MB), silica flour (SF), and microcellulose (MC), under room temperature (RT). Through detailed NMR porosity and pore size distribution analyses over extended periods, this study investigates how these additives influence the cement matrix's densification, pore refinement, and overall porosity reduction. The porosity of class H neat and class H with 10% fly ash was studied. Furthermore, porosity of class G cement with varying percentages of fly ash additive under high-temperature conditions was also investigated. Additionally, geopolymer samples were evaluated as an alternative binder system, offering a comparative baseline for traditional formulations. The findings highlight the role of temperature, additive type, and proportion in determining cement matrix performance, which is essential for applications such as wellbore integrity in oil and gas or geothermal operations.

2 Literature Review

2.1 Introduction to Cement

Cement plays a crucial role in the construction and oil and gas industries. In construction, cement-based materials have been used for centuries, with ongoing efforts to improve sustainability and reduce environmental impact (Pöllmann et al., n.d.). In the oil and gas sector, cement is essential for well construction and integrity (Kumar et al., 2022).

Manufacturing of cement is done by drying calcareous and argillaceous rocks and then grinding and mixing them in various proportions by a dry or wet process. The product is then heated to around 1426°C to 1540°C (2600°F to 2800°F) to produce clinkers. When these clinkers have cooled, they are ground to a powder and mixed with other ingredients, such as gypsum, to produce Portland cement (Nelson, 1990). The term "Portland cement" comes either from its resemblance to Portland stone or because it is a useful substitute for that type of stone.

Portland cement is mixed with other substances in order to be utilized in specific ways, creating the following mixtures:

- Concrete: a mixture of cement powder, water, and both fine and coarse aggregate such as sand, gravel, or crushed stone like limestone or granite.
- Cement paste: the mixture of cement powder and water, also known in civil engineering as grout or in petroleum engineering as cement slurry.
- Mortar: a composite material comprised of cement powder, water, and fine sand, frequently incorporating a plasticizing agent such as hydrated lime or an organic wetting agent.

Oilfield cement is produced based on the API laid down in the specification. There are six types of cement and three grades available, such as ordinary-O, moderate sulfate-resistant-MSR, and

high sulfate-resistant-HSR. The classification of cement is specified below (American Petroleum Institute, 2010):

- Class A: used in general applications when special characteristics are not required. The permitted depth is up to 6,000 feet. It is available only in O grade.
- Class B: designed for use in moderate or high sulfate resistance (HSR) and the maximum depth permitted is up to 6,000 ft of depth.
- Class C: Applied where high early strength is needed, with higher C_3A content. Also, for depths up to 6,000 ft.
- Class D: For depths from 6,000 to 10,000 ft, for moderately high temperatures and pressures. It is available in HSR and MSR grades.
- Classes G and H: The materials in their conventional form can be used as basic well cements, or they can be modified with additives to suit a wider range of well uses. Both classes are available in grades MSR and HSR.

2.2 Overview of Cement Chemistry and Hydration Processes

Portland cement is a complex inorganic material composed primarily of calcium silicates, aluminates, and aluminoferrites. Portland cement's main components - tricalcium silicate (C_3S), dicalcium silicate (C_2S), tricalcium aluminate (C_3A), and tetracalcium aluminoferrite (C_4AF) - play crucial roles in hydration and strength development. The hydration of these compounds form calcium silicate hydrate (C-S-H) and calcium hydroxide, contributing to concrete's strength and durability (Lavagna & Nisticò, 2023). C_3S and C_2S are primary contributors to strength, with C_3S hydrating faster than C_2S. C_3A and C_4AF influence early hydration and setting (Puertas et al., 2011).

In cement, water is mixed at different ratios, depending on the recommendations of the manufacturer, and the process of hydration starts. In this process, the clinker phases react with water to form hydrates and hydroxides that give strength to the cement but also generate internal porosity simultaneously. Wait-on-cement, time-water-to-cement ratio, cement composition, and the use of additives are all factors affecting the time required for the cement to attain at least a minimal compressive strength of approximately 3.5 MPa or 500 psi. Inasmuch as both Portland and oilfield cements are hydraulic cements, both types can set and harden in either dry or wet conditions, whether the slurry is exposed to air or is submerged underwater (Nelson, 1990).

The hydration of Portland cement results in mechanical bonding, heat generation, and changes in the cement paste's volume, depending on the curing conditions (Aïtcin and Flatt, 2016). Since hydrating cement is not volumetrically stable, cement pastes may lose between 1% and 8% of their total volume during curing, a process known as chemical (Le Chatelier's) contraction (Aïtcin & Robert J. Flatt, 2016; Keating et al., 1989). Powers, (1958) quantitatively studied cement hydration and determined that a water-to-cement (w/c) ratio of at least 0.42 is required for full hydration. Water in the cement can be categorized as reactive, forming a "solid gel" that contributes to the cement's bonding properties, and non-reactive ("gel water"), which is bound to the hydrated cement paste. Hydration can occur in two systems: one closed to external water sources and one open to an external water supply (Powers, 1958). **Figure 5** illustrates the chemical contraction modeled for a sample with a 0.42 w/c ratio, showing that when hydration occurs in a dry environment, the volume of air increases over time. In contrast, when hydration occurs in an open, wet environment, water infiltrates the sample through its pore network.

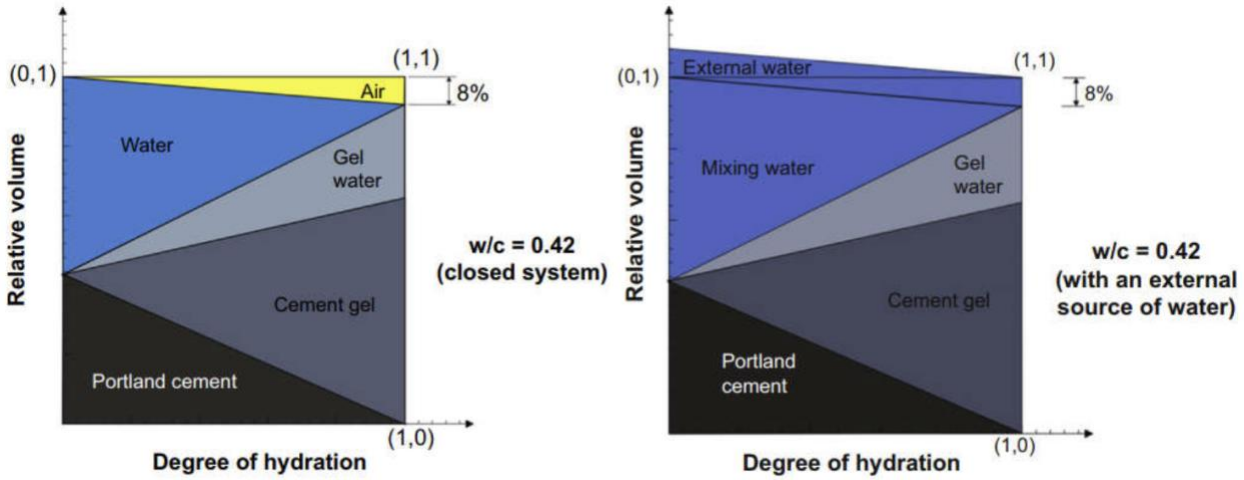

Figure 5: Changes in the Relative Volume of Cement Components During Hydration in a Dry Environment (Left) and Submerged in Water (Right) (Aïtcin and Flatt, 2016)

When Portland cement is mixed with water, a series of complex chemical reactions occur, known as hydration. This process is crucial for the development of strength and other properties of the cement paste (Lavagna & Nisticò, 2023). The hydration of cement represents a major example of an inhibited autocatalytic reaction, or chemical clock reaction, which starts when water comes into contact with dry cement powder, as reported by Luke et al., (1995). This highlights the importance of storage conditions for cement powder. Hydration produces calcium silicate hydrate (CSH)- a gel, calcium hydroxide (CH)- a crystalline phase, trisulfoaluminoferrite hydrates (Aft), and monosulfoaluminoferrite hydrates (AFm) (Aïtcin & Robert J. Flatt, 2016).

The hydration of C_3A is crucial during the initial stages of cement hydration and significantly affects the mechanical and rheological properties. Due to the rapid reaction of C_3A with water, which can cause "flash-setting" (a result of irregular hexagonal calcium aluminate hydrate platelets forming on the clinker surface), calcium sulfate is added during the clinker production process. This addition results in the formation of ettringite:

$$C_3A+3C\underline{S}H_2+26H \rightarrow C_6A\underline{S}_3H_{32}$$

Once the sulfate is depleted, the remaining C_3A reacts with the ettringite to form monosulfoaluminate (Aïtcin & Robert J. Flatt, 2016):

$$2C_3A+C_6A\underline{S}_3H_{32}+4H->2C_4A\underline{S}H_{12}$$

Silicate hydration (the hydration of alite and belite) is the dominant reaction due to silicates being the primary components of cement clinker. This reaction proceeds through five stages: dissolution (I in **Figure 6**), induction (II), acceleration (III), deceleration (IV), and diffusion (V). The reaction outcomes are as follows (Nelson, 1990; Aïtcin and Flatt, 2016):

$$2C_3S + 6H \rightarrow C_3S_2H_3 + 3CH$$

$$2C_3S + 4H \rightarrow C_3S_2H_3 + CH$$

This leads to the precipitation of calcium silicate hydrate (CSH), an amorphous and poorly crystalline phase, and calcium hydroxide (CH), also known as portlandite, which is a crystalline phase. Tricalcium silicate (C_3S) is primarily responsible for early strength development during hydration, while dicalcium silicate (C_2S) contributes mainly to final strength development (Fink, 2015).

Dissolution (I), induction (II), acceleration (III), deceleration (IV), and diffusion (V)

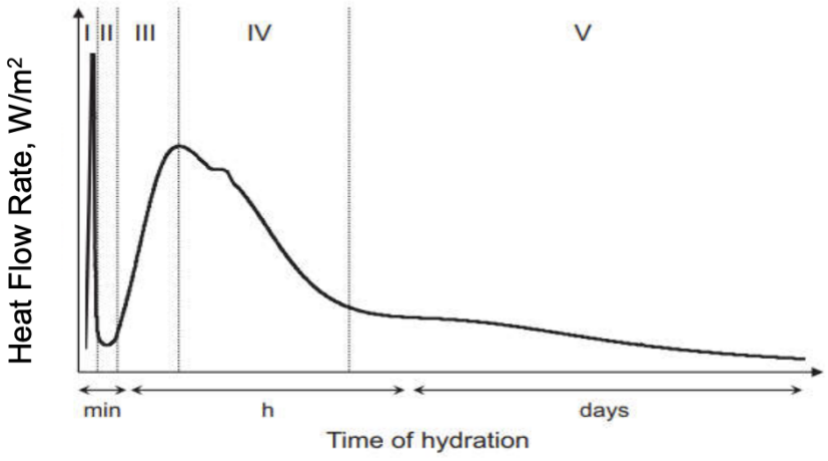

Figure 6: Heat Flow vs. Hydration Time in Cement (Aïtcin & Robert J. Flatt, 2016)

2.3 Overview of cement Additives

Additives in cement refer to those materials combined with cement aimed at altering or improving at least one of the properties that will be developed: workability, strength, durability, and many others depending on the demands of a particular application. Chemical additives in the oil and gas industry are used to alter the rate of hydration when water and cement are mixed. These additives are incorporated into cement slurries to adjust their performance to meet operational requirements (Broni-Bediako, 2016). Common chemical additives in oil well cementing include accelerators, retarders, extenders, loss circulation additives, and dispersants, among others (Roshan, 2010).

- Accelerators: These chemical additives are used to hasten the thickening time of cement, promoting faster development of early compressive strength. Common accelerators include calcium chloride and sodium chloride.
- Retarders: These additives slow down the hydration of cement, resulting in a slower development of compressive strength. Examples of retarders include lignosulfonate, cellulose derivatives, and hydroxycarboxylic acids.
- Extenders: Materials or chemicals used to reduce the density of the cement mixture, which in turn lowers its hydrostatic pressure. Bentonite and sodium silicate are commonly used extenders in the oil and gas industry.
- Heavy-weight agents: These additives have a higher specific gravity than cement, uniform particle size, and low water requirements, allowing them to control high formation pressures. Hematite and ilmenite are often used for this purpose.
- Fluid loss additives: Used to decrease the rate at which water is lost from the cement to the surrounding formation due to differential pressure. Hydroxyethyl cellulose is a commonly used fluid loss additive.

- Dispersants: These additives enhance the flow properties of cement slurries, helping to counteract high viscosity and prevent gelling in some slurries.

The strength of hardened cement paste can be enhanced, and its density reduced through the use of pozzolanic materials containing active oxides like Al_2O_3, SiO_2, and Fe_2O_3. At room temperature, these oxides react with portlandite ($Ca(OH)_2$), which is produced during the hydration of Ordinary Portland Cement (OPC) minerals. These reactions result in the formation of calcium hydrosilicates, hydroaluminates, and other hydrates, which contribute to increasing the strength of the hardened cement paste (Šeputytė-Jucikė et al., 2016).

Fly ash, a common additive improves resistance to chloride attack and reduces porosity in cement pastes (Al-Salami, 2012). When combined with alkaline activators like sodium hydroxide and sodium silicate, fly ash can optimize compressive strength and decrease porosity in concrete (Bhatt et al., 2023). Sodium hydroxide increases early hydration rates but may retard later-age hydration and affect microstructure (Nikoloutsopoulos et al., 2021). Silica fume additions can enhance compressive strength and reduce porosity in fly ash geopolymers (Bhatt et al., 2023). Sodium sulfate activation of high-volume fly ash blends improves strength, workability, and pore structure refinement. Crystalline additives also influence the pore structure of cement mortars, affecting properties such as strength and freeze-thaw resistance (Nevřivová et al., 2018).

2.3.1 Fly ash

Fly ash, a byproduct of coal combustion, can be used as a partial substitute for Portland cement. It is classified as a "Pozzolan" material, containing silica and aluminum oxide (Bhatt et al., 2023). Approximately 750 million tons of fly ash are produced each year, posing a major disposal challenge. Although fly ash holds significant potential as an engineering material, it has not yet been fully utilized (Kabir et al., 2016).

The properties of fly ash depend on the technology used in its production. Fly ash is generated and released before the flue gases are emitted, typically through two types of boilers: fluidized bed boilers and conventional pulverized coal boilers (Kar, 2022). At present, discussions focus on coal and its different types, both of which play a critical role in determining the characteristics of fly ash (T. Matsunaga et al., 2002).

Coal-fired thermal power plants produce 60% to 88% of fly ash, which is collected using pollution control equipment like electrostatic precipitators. Fly ash is formed by burning coal at high temperatures ranging from 1200°C to 1700°C and consists of various organic and inorganic components. Due to its complex composition, diverse particle size and shape, fine nature, and composition, the identification, specification, characterization, and utilization of fly ash are challenging processes (Kar, 2022).

Study shows that the addition of fly ash to concrete mixtures can have significant effects on both porosity and strength. Fly ash reduces the porosity of cement pastes and concrete due to its small particle size, which fills voids in the concrete, resulting in a denser matrix. Concrete with high fly ash content (90-100%) exhibits smaller pores compared to conventional concrete using 100% cement (Bhatt et al., 2023). In fact, concrete mixtures with 90% fly ash experience a 76-78% reduction in porosity compared to normal concrete, depending on the molarity of the alkaline activator used. While fly ash improves certain properties, its impact on strength can vary. High fly ash content (70-100%) typically leads to lower compressive strength compared to normal concrete. The optimal use of fly ash for compressive strength is around 10% of the binder weight, with higher percentages resulting in decreased strength (Bhatt et al., 2023).

2.3.2 Class F fly ash

The American Society for Testing and Materials (ASTM) classifies fly ash into two categories: Class C fly ash (high calcium) and Class F fly ash (low calcium). Low calcium fly ash is widely used due to its availability and technical advantages, including reduced heat of hydration, bleeding, segregation, permeability, and improved resistance to sulfates and acids. However, there are some disadvantages associated with low calcium fly ash in concrete, such as reduced carbonation resistance and increased water absorption (Rashad, 2015).

2.3.3 Silica Flour

Silica flour is used principally as a very reactive pozzolanic material owing to its high content of reactive silica. When it is added to cement, it readily reacts with the calcium hydroxide that is produced during hydration to produce additional C-S-H, which is important for strength development. The pozzolanic reaction decreases the free calcium hydroxide amount within the concrete matrix, which improves long-term durability by enhancing sulfate resistance, reducing permeability, and reducing negative effects caused by the alkali-silica reaction (Mehta, 1986).

The pozzolanic activity of silica flour increases, in general, the compressive strength of cement by making the arrangement denser and more compact, while spaces in the matrix of cements are occupied by minute-size silica flour particles (Ramachandran, 1995). Silica flour is added to increase the durability of concrete by reducing the permeability of the cement paste, which protects it from the penetration of harmful substances, such as chloride ions and sulfates (Neville, 2011). The application of silica flour is particularly useful in an environment where long-term strength is required, such as marine structures and oil production platforms. Silica flour imparts chemical resistance to the cement against aggressive environmental conditions. Moreover, the reduced

content of calcium hydroxide increases the cement's resistance to acidic and sulfate-rich environments, thus increasing the life of concrete elements (Dodson, 1990).

Silica flour is also extensively used in the oil and gas industry in the cementing of deep wells that are characterized by high temperature and pressure. The addition of silica flour to cement counteracts the retrogression of the strength of the cement, a process wherein the onset of high temperatures in cement leads to a loss of mechanical integrity (Nelson & Guillot, 2006). Silica flour increases the heat resistance of oil well cement and reduces the formation of harmful crystalline phases that seriously affect the structural integrity of the cement. The pozzolanic reaction involving silica flour can be expressed as:

$$SiO_2+Ca(OH)_2+H2O \rightarrow C\text{-}S\text{-}H$$

This chemical reaction describes how in water, SiO_2 reacts with $Ca(OH)_2$ to form C-S-H, which is the main product responsible for strength in cement-based materials. The ability of silica flour to become more reactive can be attributed to the smaller size of its particles, thereby increasing the surface area available for pozzolanic activity leading to quicker strength development.

2.3.4 Microcellulose

Microcellulose is a highly subdivided form of cellulose that, with increasing interest, is being used as an additive in cementitious composites to enhance several properties: workability, strength, and durability. Cellulose, a natural polymer derived from plant materials, through methods such as mechanical milling or chemical processing, yields microcellulose. Due to its huge surface area and fibrous arrangement, microcellulose exerts several positive effects in cement-based formulations. The reinforcing action of microcellulose in cement-based composite enhances the mechanical properties of the matrix. In addition, microcellulose fibers once added to cement form a network that enhances the aggregation of cement particles and leads to high cohesion, reducing bleeding

during the curing process. The improvement in crack resistance of cement is due to its fibrous structure, which acts as micro-reinforcement and contributes to reducing shrinkage, increasing the tensile strength (Filho et al., 2021).

The addition of microcellulose increases the viscosity of cement slurries, improving workability and stability, especially when the water-to-cement ratio is low. Acting as a water-retention agent, microcellulose prevents extreme loss of mixing water during the curing process, which helps to control the setting times and reduces the chance of drying out too early (Ardanuy et al., 2015).

One of the most important properties of microcellulose in cementitious materials involves its shrinkage-reducing ability. Shrinkage is often developed through the evaporation of water during the hydration process and can lead to crack development in the hardened cement. The fibrous nature of microcellulose helps mitigate these effects due to the improved distribution of internal stresses, which prevents crack propagation (Barabanshchikov et al., 2021). This has many beneficial applications in high-performance concrete where crack resistance is a major factor.

The incorporation of microcellulose enhances the durability of concrete over extended periods. By decreasing the porosity of the cement matrix, microcellulose restricts the penetration of detrimental substances, including chlorides and sulfates, which are capable of causing degradation with time. Consequently, microcellulose proves to be especially advantageous in settings subjected to harsh chemicals or freeze-thaw cycles (Filho et al., 2021).

Microcellulose is an environmentally friendly additive due to its derivation from natural sources. Derived from renewable plant materials, its use in cement aligns with the increasing demand for green construction materials. In addition, microcellulose can reduce the total amount of cement in a mixture, which, in turn, can reduce carbon dioxide emissions associated with the production of cement (Mohammadi et al., 2017).

It works mainly by affecting the rheological and microstructural properties of the paste. The presence of fine particles, in addition to the fibrous nature of microcellulose, increases the viscosity of the mix, hence improving its flow behavior. During hydration, the fibers of microcellulose interact with cement particles, yielding a dense matrix that reduces bleeding and segregation as well as the formation of large cracks. This will result in a denser and more homogeneous structure with improved mechanical properties (Filho et al., 2021).

Microcellulose adds significant value to cement by improving mechanical properties, controlling shrinkage, enhancing durability, and promoting sustainability. In particular, it proves very effective for high-performance applications that require crack resistance and long-lasting durability.

2.3.5 Microblock

Microblock is a specialized additive that enhances the properties of cement-based materials, both mechanically and chemically. Incorporating microblocks into cement or concrete mixtures alters the setting and hardening process to improve specific characteristics, such as strength, durability, and resistance to environmental factors. These additives comprise carefully engineered microblocks that interact positively with the hydration reaction, resulting in enhanced performance in both fresh and hardened states (Elkem, 2024).

The incorporation of microblocks into concrete significantly enhances its compressive strength by refining its microstructure, reducing voids, and strengthening cement-aggregate bonds, ultimately producing a stronger, more durable material. By decreasing cement paste porosity, Microblock significantly improves resistance to water and chemical damage, making it a crucial component in structures that demand long-term durability, such as marine infrastructure and chemical facilities (Elkem, 2024).

Microblock enhances cement's thermal resistance, making it suitable for high-temperature applications like oil wells and industrial settings. This improvement ensures long-term structural stability under extreme temperatures (Matsunaga et al., 2002)

2.4 Overview of geopolymer

Geopolymers are eco-friendly, inorganic polymers formed from aluminosilicate materials and alkaline activators. With a lower carbon footprint and superior properties, they offer a sustainable alternative to traditional Portland cement, leveraging silica and alumina from natural sources and industrial byproducts.

2.4.1 Geopolymer Formation

Geopolymer production involves dissolving aluminosilicate materials in a strong alkaline solution, typically using sodium or potassium hydroxide as the catalyst. This process triggers the release of silica and alumina compounds, which then undergo a polycondensation reaction to form a robust, three-dimensional network of aluminosilicate gel. As this gel hardens, it creates the binding agent that characterizes the geopolymer (Davidovits, 2008; Duxson et al., 2007). The general chemical reaction can be represented as:

$$n(Si_2O_5, Al_2O_2)+mH_2O \rightarrow (Na,K)[(SiO_2)z(AlO_2)y]+H_2O$$

This network structure imparts exceptional chemical stability and durability to the geopolymer matrix.

2.4.2 Benefits of Geopolymers

- Environmental Sustainability: One of the primary advantages of geopolymers is their lower environmental impact compared to traditional cement. Portland cement production is highly carbon-intensive, accounting for approximately 5-8% of global CO_2 emissions

(Davidovits, 2008). Geopolymers, on the other hand, can reduce CO_2 emissions by up to 80% since they do not require high-temperature kiln processes for production. Instead, geopolymers are synthesized at room temperature using industrial byproducts like fly ash and slag (Duxson et al., 2007).

- High Strength and Durability: Geopolymers exhibit excellent mechanical properties, including high compressive strength that can exceed that of Portland cement. Studies have shown that geopolymer concretes can achieve compressive strengths of up to 100 MPa, depending on the mix design and curing conditions (Provis & van Deventer, 2009). Additionally, geopolymers have superior resistance to chemical attack, particularly in acidic and sulfate-rich environments, due to their low calcium content and dense microstructure.
- Low Shrinkage and Improved Durability: Geopolymers exhibit low shrinkage during curing, which reduces the risk of cracking and enhances the long-term durability of structures. The dense microstructure of geopolymers also contributes to their resistance to water ingress and freeze-thaw cycles, making them ideal for use in harsh environments (Provis & Bernal, 2014).

2.4.3 Challenges and Limitations

While geopolymers offer numerous advantages, there are some challenges that need to be addressed:

- Alkaline Activator: The use of highly alkaline activators, such as sodium hydroxide, poses safety concerns during handling and increases the cost of geopolymer production. Researchers are exploring alternative, less hazardous activators to improve the viability of geopolymers for large-scale applications (Provis & Bernal, 2014).

- Standardization: Unlike Portland cement, which has well-established standards for its use and performance, geopolymers lack standardized mix designs and guidelines. More research and development are needed to create comprehensive specifications for geopolymer use in construction and industrial applications.

Geopolymers present a promising, sustainable alternative to traditional cementitious materials, offering superior strength, durability, and environmental benefits. Their applications in construction, waste management, and industrial processes continue to expand as research and development in this field progress.

2.5 Cement porosity and well integrity

The term "cement porosity" describes the existence of microscopic holes or pores in the cement matrix, which can have a big impact on the material's strength, permeability, and durability. Since excessive porosity can increase permeability, managing porosity is essential to ensure the cement offers appropriate zonal isolation in well cementing. High porosity cement can impair the seal between the wellbore and casing because it is more prone to fluid movement. Severe well integrity problems could arise from this, including constant casing pressure, annular pressure accumulation, and possibly leaks into nearby formations or to the surface (Nelson & Guillot, 2006).

Porosity is essential to a well's long-term integrity. Increased permeability from high porosity makes it easier for gases, oil, or water to pass through the cement matrix, which can lead to the failure of zonal isolation and the loss of well control (Goodwin & Crook, 1992). Poor cement performance, often caused by excessive porosity, can lead to sustained annular pressure (SAP), a prevalent well integrity issue. This occurs when hydrocarbons or other fluids migrate into the annular space and build pressure over time, eventually leading to well control problems (Bois et al., 2012).

Furthermore, the consequences of porosity may be increased by the interaction between the cement and the downhole environment, especially when high pressure and temperature (HPHT) conditions are present. Cement in HPHT wells may undergo heat degradation. When this happens in conjunction with high porosity, the cement's strength and integrity may be further compromised, increasing the likelihood of cracking or debonding. This may result in the development of fluid movement channels and micro-annuli (De Andrade & Sangesland, 2016). As a result, lowering cement porosity is critical for increasing its resistance to mechanical loads and assuring the long-term effectiveness of wellbore sealing (Safiuddin & Hearn, 2005).

The use of additives such as silica flour and micro-silica has been found to minimize cement porosity, hence enhancing its mechanical qualities and durability. These additives fill spaces within the cement matrix, resulting in a denser, more impermeable structure, reducing the chance of fluid migration and improving well integrity (Zhang & Bachu, 2011). Ensuring low porosity by careful cement formulation and the application of appropriate additives is thus a critical approach for sustaining well integrity, especially in difficult situations like HPHT wells or wells with complicated formations.

2.5.1 Long-term Porosity Evolution

Long-term porosity evolution in cement is influenced by continued hydration, carbonation, and environmental exposure. Cement pastes show changes in open porosity characteristics over time due to hydration progress and carbonation (Tracz & Zdeb, 2019). Carbonation can lead to a loss of gel and capillary nanopores, resulting in reduced porosity and permeability (Cheshire et al., 2017). The complex pore system in cement paste, ranging from nanometers to millimeters, significantly affects properties like strength, shrinkage, and permeability (Jennings et al., 2008). Exposure to CO_2 under high temperature and pressure conditions can increase cement's resistance

to carbonic acid attack. Environmental drying can cause coarsening of pores in cement paste (Soja et al., 2020). In limestone calcined clay cement, long-term hydration leads to continued reactions and changes in phase assemblage and porosity (Cheshire et al., 2017). These porosity changes impact cement durability and performance over time.

2.5.2 Methods Used for Measurement of Cement Porosity

Methods for measuring cement porosity in the oil and gas industry include various techniques, each suitable for specific applications and possessing unique strengths:

- Mercury Intrusion Porosimetry (MIP): This is a commonly used technique for assessing cement porosity in the oil and gas industry. This method involves applying increasing pressure to force mercury into the pores of a cement sample. The data collected from mercury intrusion are then used to determine the pore size distribution. Despite its widespread use, MIP is considered a destructive testing method because the high pressures applied during the procedure can lead to structural changes in the cement, such as collapsing pores. While MIP excels in measuring small pore sizes, it may not be ideal for materials with interconnected pores due to potential inaccuracies caused by the "ink-bottle effect"—a phenomenon where narrow connections between larger pores can distort the measurements (PennState Materials Research Institute, n.d.).
- Helium Pycnometry: This involves using helium gas to measure the volume of solid particles within a cement sample, which enables the calculation of the sample's total connected porosity. Since the method does not alter the sample, it is considered non-destructive, making it suitable for situations where maintaining the integrity of the sample is crucial. This technique is especially valuable for applications requiring high precision in measuring the volume of connected pores (Unosson et al., 2015).

- Scanning Electron Microscopy (SEM): For this method, the preparation process involves drying, polishing, and coating cement samples with a conductive material such as gold or carbon. These steps inevitably alter the original microstructure of the cement, making SEM a destructive method for porosity analysis. Although SEM doesn't measure porosity directly, it produces high-resolution images that allow for detailed examination of changes in the microstructure and pore characteristics (Jarrahi et al., 2019).
- Gas Adsorption Techniques: Techniques such as Brunauer-Emmett-Teller (BET) analysis, measure the surface area and pore volume by adsorbing gases like nitrogen onto the surface of a cement sample. The preparation process for these methods often involves steps like drying or degassing, which can affect the microstructure of the sample and potentially alter the resulting porosity measurements. While these techniques provide valuable insights into pore characteristics, the sample preparation may introduce changes that affect the accuracy of the analysis (Medina-Rodriguez & Alvarado, 2021).
- Thermogravimetric Analysis (TGA): This technique measures the loss in weight of a sample as it is heated to high temperatures, causing components such as water and carbonates to evaporate. The process fundamentally alters the structure and composition of the cement, making TGA an inherently destructive method (Llorens et al., 2023).
- Water Saturation Techniques (Boiling Water Saturation): This approach involves submerging cement samples in boiling water to determine pore volume. The exposure to heat and moisture can create microcracks or cause other structural changes in the cement, rendering the method semi-destructive due to the potential alterations in the sample's original state (Chu et al., 2021).

Most traditional methods for measuring cement porosity in the oil and gas industry are considered destructive because they alter the sample's microstructure or integrity during the testing process. Given the limitations, there is an increasing need for non-destructive techniques to preserve the sample's original properties while still providing accurate porosity measurements.

2.6 NMR Technology for Porosity Assessment

Nuclear Magnetic Resonance (NMR) technology has become an invaluable tool for characterizing porosity in rock formations. NMR measures the relaxation of polarized nuclei, providing crucial information about pore structure and fluid content (Guo et al., 2020). This non-destructive technique allows for rapid analysis of core samples without prior preparation. NMR can determine porosity, pore size distribution, permeability, and capillary pressure (Amani et al., 2017). Mobile NMR devices, such as the NMR-MOUSE, enable on-site core analysis. Low-field NMR has shown promise in distinguishing between primary and secondary porosity in carbonate reservoirs (Mai & Kantzas, 2002). The technology can also identify multiple fluid types within pore spaces and assess oil viscosity (Amani et al., 2017). Recent advancements utilize susceptibility-induced internal field gradients to probe porous media microstructure. Overall, NMR has significantly enhanced formation evaluation in the petroleum industry (Amani et al., 2017).

2.6.1 Principles of NMR

In petroleum engineering, NMR techniques such as nuclear magnetism, polarization, T_1 and T_2 relaxation times, pulse tipping, free induction decay, spin echoes, and CPMG sequences are employed to analyze fluids within the pore spaces of rocks. These principles allow for determining porosity and its distribution independent of mineralogy (Coates et al., 1999). Additionally, NMR is used for estimating irreducible water saturation, identifying hydrocarbon types, assessing oil

viscosity, and predicting rock permeability, provided appropriate calibration is performed (Dunn, Bergman, & Latorracca, 2002).

In their ground state, many atomic nuclei exhibit continuous spinning around their axis, resulting in spin angular momentum and an associated intrinsic magnetic moment that align in the same direction, thus creating nuclear magnetism. The hydrogen proton, which is the focus of ^{1}H proton NMR, possesses a spin of 1/2, enabling the phenomenon of nuclear magnetic resonance (Dunn, Bergman, & Latorracca, 2002). The widespread use of ^{1}H NMR in both laboratory and field applications is due to the high abundance of hydrogen in formations that contain water and/or hydrocarbons.

Polarization is the initial step in an NMR measurement, involving the alignment of magnetic nuclei with an externally applied static magnetic field. When this field is introduced, it exerts a torque on the nucleus, prompting the nuclear spin axis to align with the direction of the field. The low-energy state corresponds to the parallel alignment of the proton with the static field, while the high-energy state corresponds to an anti-parallel alignment. Because more spinning protons favor the lower energy state, the overall magnetic moment of the protons aligns parallel to the external magnetic field (Minja & Lieberman, 2017). Due to the torque exerted by the external field, the axis of the nucleus undergoes a motion called precession, which occurs at the Larmor frequency. This frequency is calculated by multiplying the static magnetic field strength by the gyromagnetic ratio ($\gamma/2\pi$ = 42.58 MHz/T for hydrogen nuclei). The Larmor frequency is influenced by the strength of the static magnetic field and the specific nuclear species, allowing the operational frequency to determine the location of the region being examined (Coates et al., 1999). Once the protons reach equilibrium with the external magnetic field, B_0, an applied radiofrequency (RF) pulse disrupts this equilibrium, causing the protons to lose their alignment with the field. Following the RF pulse,

the nuclei realign and continue to precess around B_0. The polarization process is time-dependent and can be described by:

$$M_z(t) = M_o(1 - e^{\frac{-t}{T_1}}) \qquad \textit{Equation 1}$$

The time (t) of exposure of protons to the magnetic field (B_o) is represented in the polarization process, where $M_z(t)$ denotes the magnitude of magnetization at a given time, M_0 is the maximum magnetization attainable in a specific magnetic field, and T_1 is the longitudinal relaxation time, also known as the spin-lattice relaxation time. T_1 characterizes both the spin system and its environment, indicating how efficiently the magnetic energy of the spin system is transferred to or from the surroundings. A higher T_1 value suggests weak coupling and slower energy transfer, while a lower T_1 indicates stronger coupling and a quicker return to equilibrium (Dunn, Bergman, & LaTorraca, 2002). The next phase in the NMR measurement process is pulse tipping, which shifts the magnetization from the longitudinal axis to the transverse plane (from the z-axis to the xy-plane). This is achieved by applying an oscillating magnetic field (B_1) perpendicular to the static magnetic field (B_0), causing the protons to transition from lower to higher energy levels. The result is that the protons begin to precess in unison, producing nuclear magnetic resonance (Coates et al., 1999).

When the transverse magnetic field is switched off, the protons begin to lose their phase coherence, resulting in a decrease in net magnetization. This diminishing signal is recorded by a receiver coil and is known as Free Induction Decay (FID). The FID typically follows an exponential decay pattern with a short time constant (T_2^*), due to variations in the B_0 magnetic field, causing protons in different locations to precess at different Larmor frequencies.

The loss of phase coherence can be corrected by applying a 180° pulse (B_1), which reverses the dephasing and leads to Spin-Echo Detection. The time constant associated with the decay of

transverse magnetization is called the transverse relaxation time (T_2). The spin-echo signal magnitude over time can be described by an exponential function that characterizes the decay process.

$$M_x(t) = M_{ox}(1 - e^{\frac{-t}{T_2}}) \qquad \textit{Equation 2}$$

The strength of the detected magnetic field depends on the number of protons that remain aligned within the transverse (T_2) plane, which decreases as measurement time increases (typically on the order of milliseconds). This reduction occurs because 180° pulses cannot realign protons that have moved out of the plane or have relaxed due to factors like Brownian motion and surface relaxation T_2. As pore size decreases, the likelihood of a proton interacting with the surrounding surface increases, resulting in shorter relaxation times for water in smaller pores compared to larger ones. When surface relaxivity is the predominant factor, T_2 is directly proportional to pore size, with the relationship defined by the equation below.

$$\frac{1}{T_2} = \rho_r \frac{S}{V} = \frac{\rho_r}{a} \qquad \textit{Equation 3}$$

Here, ρ represents the surface relaxivity (μm/s), A is the surface area (m^2), V denotes the pore volume (m^3), and a refers to the characteristic pore dimension, typically the radius (r). A comparable relationship also applies to spin-lattice relaxation (T_1).

T_1 and T_2 measurements involve encoding frequency at a constant gradient value while varying the time. Another NMR approach is phase encoding, which adjusts gradient values with a fixed encoding time, making it effective for imaging samples with short relaxation times (Muir & Balcom, 2012). Single Point Ramped Imaging with T1 Enhancement (SPRITE), introduced by Balcom et al. (1996), utilizes a brief RF pulse and a ramped gradient to generate images of samples with short T_2^*, serving as an alternative to the Single Point Imaging (SPI) technique, which relies on strong, rapidly switched gradients. The Double Half k-space (DHK) SPRITE experiment is

used for one-dimensional imaging, where k-space represents a matrix of spatial frequency data in the NMR image before Fourier transformation. In DHK SPRITE, data for one-half of k-space are collected by incrementing the gradient, followed by a relaxation delay of 5 X T_1, after which the second half of k-space is sampled by reversing the gradient increments. The resulting data sets are combined into a single linear array, and the two k = 0 points are averaged before performing a Fourier transform (Muir & Balcom, 2012).

2.6.2 Application of NMR in Cement Studies

Nuclear Magnetic Resonance (NMR) has been extensively used to study cement porosity, hydration, and microstructure. NMR can measure pore size distribution, water interactions, and C-S-H gel development. It has been applied to various cement types, including oilfield cements, with studies spanning from minutes to over a year of hydration (Saleh et al., 2021). NMR relaxometry has revealed the formation of nano and sub-nano structures in C-S-H gel, supporting the Jennings colloidal model. Researchers have used NMR to determine cement density, composition, and desorption isotherms (Muller et al., 2013). Two-dimensional NMR techniques have provided evidence of water exchange between gel and capillary pores. NMR cryoporometry has been employed to study pore size distribution and the effects of additives on cement porosity (McDonald et al., 2010). These studies demonstrate NMR's versatility in non-destructively characterizing cement microstructure and properties.

2.6.3 Advantages of NMR over Other Methods

Nuclear Magnetic Resonance (NMR) offers several advantages over other porosity measurement techniques. NMR provides superior porosity and pore size distribution measurements compared to conventional methods (Zhu et al., 2019). It is non-invasive, considers the entire sample volume, and eliminates user bias in the field of view selection. NMR cryoporometry can characterize

nanoporous structures in shales more effectively than gas sorption, mercury intrusion porosimetry (MIP), or electron microscopy (Zhu et al., 2019). Unlike MIP, NMR does not risk damaging the sample structure under high pressure. NMR also shows an excellent correlation with measured cake thickness in drilling fluid infiltration studies (Bageri et al., 2021). NMR relaxometry measurements agree well with mercury intrusion and retention curves for determining pore size distribution and hydraulic properties (McDonald et al., 2010).

2.7 Limitations of Traditional Porosity Measurement

Recent research highlights the challenges in accurately measuring porosity in cement-based materials due to their complex, multiscale structure that changes over time (Jennings et al., 2008). Traditional methods face limitations in capturing long-term changes, prompting the development of new techniques. X-ray computed tomography offers non-destructive 3D insights into microstructure (Brisard et al., 2020), while dual CT scans can characterize interfacial transition zones. Neutron imaging has been used to study time-resolved porosity changes at cement-clay interfaces (Shafizadeh et al., 2020). Other methods include helium pycnometry, mercury intrusion porosimetry, and water saturation (Tracz & Zdeb, 2019). Nitrogen and water vapor sorption, proton NMR, and small-angle scattering are also employed to characterize micro- and nano-scale pores. Researchers emphasize the importance of combining multiple techniques to obtain more accurate measurements (Tracz & Zdeb, 2019), as porosity significantly influences cement properties and durability.

3 Materials and methods

3.1 Sample Preparation

The initial phase in sample preparation involves precise measurement of material weights utilizing a digital balance. In the initial set of experiments, a precise weighing of the materials was done, starting with 792 grams of class G cement and 348 grams of distilled water, which is going to produce 600 ml of cement slurry, establishing the control samples for this research. The materials used in this experiment were prepared by mixing various quantities of Class G cement with different additives, such as fly ash (FA), microcellulose (MC), microblock (MB), and silica flour (SF), in specific proportions. Each sample was mixed with distilled water to create cement mixtures for testing.

Class G was used as the base materials, with some samples containing either 5%, 10%, or 20% fly ash (FA) to study the effects of this additive on cement properties. Microcellulose (MC), Microblock (MB), and silica flour (SF) were also incorporated into separate samples at 10% or 5% concentrations. Similarly, class H cement neat and with 10% fly ash was prepared essentially using the outlined method. Additionally, a geopolymer sample was prepared using a confidential recipe. The total weight of the components (distilled water, cement, and additives) was carefully measured for each mixture, and the combinations were designed to analyze the effects of these materials on the performance of the cement, particularly in relation to hydration, strength, and porosity.

Table 1: Summary of the composition of the various cement formulations

Sample	Distilled water (grams)	Class G cement (grams)	Fly ash (grams)	Microcellulose (grams)	Microblock (grams)	Silica Flour (grams)	Class H cement (grams)
Class G	348	792	-	-	-	-	-
Class G + 5% FA	348	792	39.6	-	-	-	-
Class G + 10% FA	348	792	79.2	-	-	-	-
Class G + 20% FA	348	792	158.4	-	-	-	-
Class G + 10% SF	348	792	-	-	-	79.2	-
Class G + 5% MC	348	792	-	39.6	-	-	-
Class G + 5% MB	348	792	-	-	39.6	-	-
Class H	326	-	-	-	-	-	860
Class H + 10% FA	326	-	86	-	-	-	860

Secondly, once all the materials have been measured, the handling diverges based on the experiment set. In the first set of samples, the material remains in its original state. For the second set of samples, a manual mixing process is initiated, where the class G cement and additives, and class H and additive are blended by hand until homogeneity. Once all the respective procedures are done the material is poured into the mixer **Figure 7**.

Figure 7: Laboratory mixer used for mixing cement slurry

Subsequently, the mixer is promptly initiated, and within the initial 15 seconds, the neat class G and H cement or the pre-blended mixture is carefully added into the mixer set at a shear rate of 4000 RPMs. Just before the laps of the 15 seconds, the top of the lid is closed, for the following high shear mixing at 12000 RPMs that last 35 seconds. Once the stipulated mixing time concludes, the cement slurry is poured into a pipe **Figure 8**.

Table 2: Dimensions of each sample tested

Sample	Length of Sample (cm)	Diameter of Sample (cm)
Class G	10.82	2.54
Class G + 5% FA	12.87	2.54
Class G + 10% FA	10.95	2.54
Class G + 20% FA	13.21	2.54
Class G + 10% SF	13.32	2.54
Class G + 10% MC	11.37	2.54
Class G + 5% MB	13.24	2.54
Class H	12.58	2.54
Class H + 10 FA	12.57	2.54
Polymer	24.20	2.54

Figure 8: Customized pipes used for curing the cement samples

Following the molding, the cement is carefully immersed in water baths, that can be at room temperature or maintained at an elevated temperature of 75°C, as depicted in **Figure 9.** The submersion of the samples initiates the curing process, allowing the samples to garden adequately within the molds.

Once the desired curing period is reached, the samples are removed from the water baths and prepared for testing. The samples undergo Nuclear Magnetic Resonance (NMR) testing to measure porosity, with care taken to ensure minimal disturbance to the samples' cured state. During testing, the samples are placed in the NMR equipment, where relaxation times are measured, providing

insights into the internal pore structure and porosity changes over time. The NMR measurements are repeated at specific intervals to monitor the evolution of porosity throughout the curing period, allowing a comprehensive assessment of the influence of additives and curing conditions on cement porosity.

Figure 9: Water bath for curing samples

3.2 Nuclear-magnetic Resonance Measurements

Nuclear magnetic resonance (NMR) became a valuable tool in physics, chemistry, and biology since its discovery in 1946 by scientists at Stanford and Harvard universities. NMR tools for petroleum exploration were built as early as the 1960's but did not gain popularity until the beginning of the 1990's (Dunn et al., 2002). In this approach, well-logging tools are constructed as 'inside-out' NMR equipment with large static magnetic fields and high-frequency oscillating magnetic fields. The amplitude of the 1H NMR is used to estimate the porosity of the surrounding

formation (e.g. fluid content), and the relaxation times are used to evaluate the pore size distribution. When water and hydrocarbon have significantly different relaxation times, the amount of oil/gas can be estimated in situ. It has been found that the hydrostatic pressure does not have an important influence on the relaxation times of water within porous space (Barrie, 2000)

3.2.1 NMR Hardware

A common NMR setup (see **Figure 10**) consists of two superconducting magnets, shim coils, and a probe that contains the RF coils, and optional, gradient coils. Connected to a computer are a shim power supply, RF source, pulse programmer, digitizer, RF detector, and an RF amplifier. For the gradient coils, a separate amplifier and pulse programmer are used.

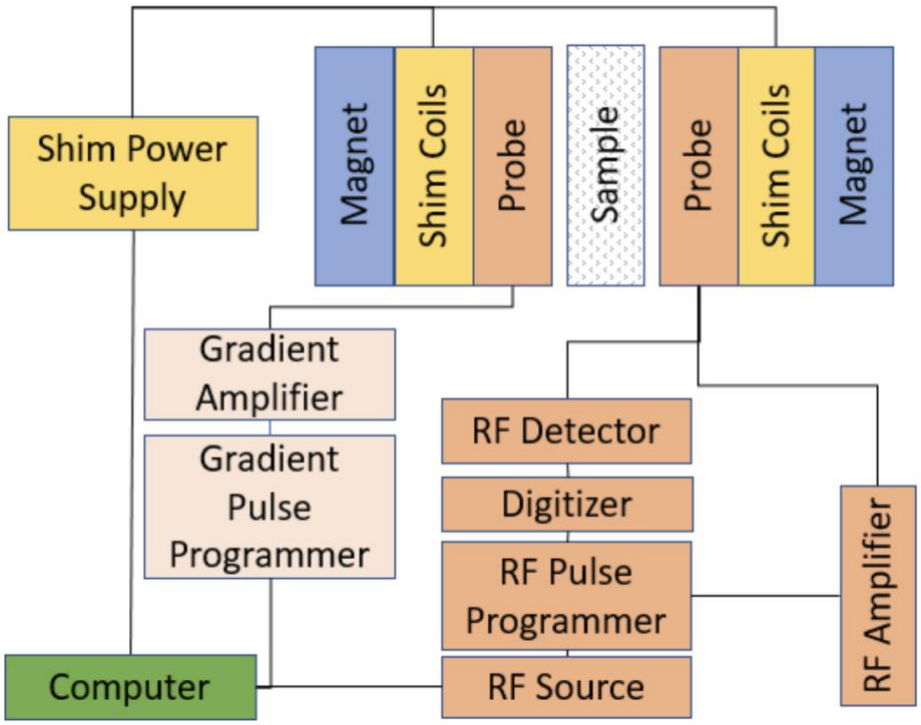

Figure 10: Typical NMR System Components, adapted after (Hornak, 2017)

3.2.2 NMR System Calibration

Before running a series of measurements, the system is calibrated with a pre-configured calibration sample with a diameter of 33 mm, length of 48 mm, 17.45 ml of NMR fluid volume, and the following properties: T_{2max} = 10ms, T_{2max} = T_{1max} = 100ms and 42.5% NMR porosity. A special tool is used to center the sample inside the magnetic field of the NMR system. To ensure accuracy at each time, the machine was calibrated each day before testing for a total of 63 times throughout the test period.

Figure 11: Calibration sample

Calibration is necessary to ensure that all tests are correctly displaying the results in units of volume or porosity. The calibration test determines the NMR resonance frequency, the resonance frequency pulse lengths for 90° and 180° tip angle pulses, and the calibration factor for all the acquisition tests (performed to convert NMR machine units to fluid volume by using the known calibration sample volume (**Figure 11**)). Moreover, a system health measurement is performed during calibration, which measures the NMR resonant frequency, the magnetic field homogeneity, the signal-to-noise ratio (SNR), the system sensitivity, and the RF probe frequency response (reflected RF power versus frequency) (Green Imaging Technologies, 2016).

An Oxford Maran NMR system was used, manufactured by Oxford Instruments (**Figure 12**). This operates at a frequency of 2 MHz, similar to NMR logging tools, and is paired with the Green

Imaging Technology (GIT) software, enabling hardware control and sample database access. Before running a series of measurements, the system is calibrated with a pre-configured calibration sample

Figure 12: Bench-top Nuclear Magnetic Resonance (NMR) device used for measuring porosity

Figure 13 below illustrates the findings from measurements conducted on two distinct samples and the influence of τ on the results over a period of up to 230 days, as reported by Ichim 2017. In this context, the τ parameter refers to the time interval between the 90° pulse and the first acquired echo. According to Ichim 2017, larger τ values result in lower measurement resolution, which leads to reduced signal acquisition from water confined within the sample's pores. For higher τ values, the signal predominantly reflects larger pores, whereas smaller τ values capture contributions from both large and small pores.

The study highlights an average difference of 14.5 porosity units between the two measurement conditions. Initially, during the first 14 days, this difference is smaller due to the larger fluid-filled pore sizes present in the cement matrix. As hydration progresses, the fluid-filled pore sizes diminish, and water is consumed in the formation of hydration products, causing the difference between the two measurement conditions to stabilize.

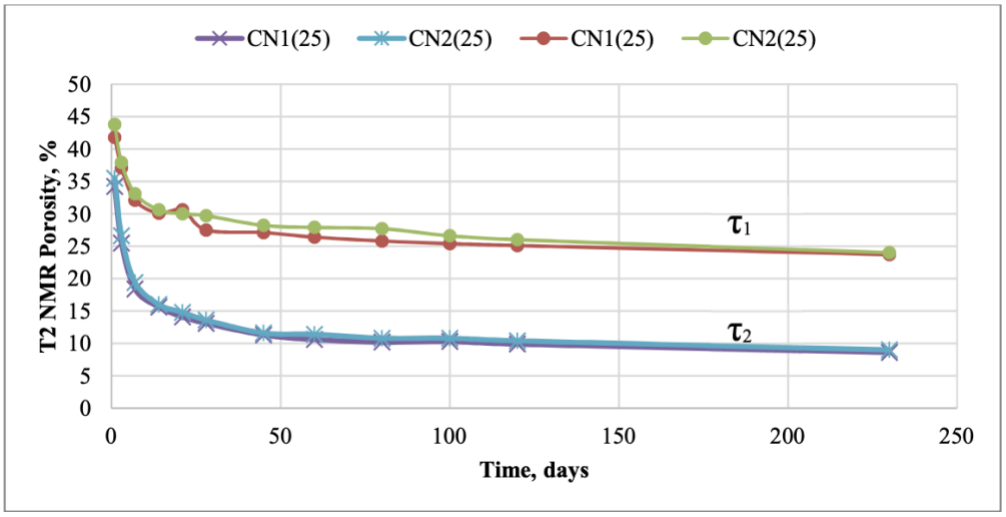

Figure 13: T2 NMR Porosity – Neat Cement – 25°C – τ_1=57 µs, τ_2=150 µs (Ichim 2017)

In the subsequent analysis, only the measurements conducted with τ = 50 µs are considered, as per the approach outlined.

4 Results

This section presents the results obtained over a test period of 146 and 35 days for samples cured at room temperature and high temperature respectively in this work. The results will be presented in figures.

4.1 Class G-neat

The porosity of neat class G cement at room temperature was found to be 30% by day 1. **Figure 14** shows the NMR porosity of Class G-neat cement over 146 days cured under room temperature (RT) conditions. The trend of both samples constantly shows a decrease in porosity with time. A strong decline within the first 20 days and stabilization after approximately 80 days, achieving a plateau near 15%. It is seen that between day one and eleven, the steepest drop is observed for this sample leading to a final porosity value of 16% by day 146. **Figure 15** provides a detailed view of porosity at various time intervals over the 146 days. It highlights the steady decline in porosity during early curing, followed by stabilization in the later stages of hydration.

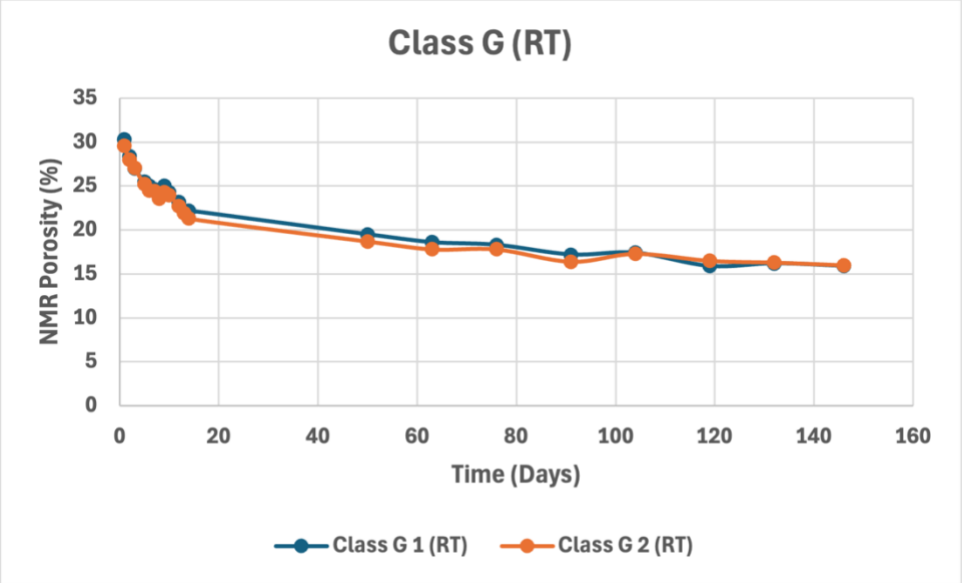

Figure 14: NMR Porosity Over Time for Class G Cement at Room Temperature (RT)

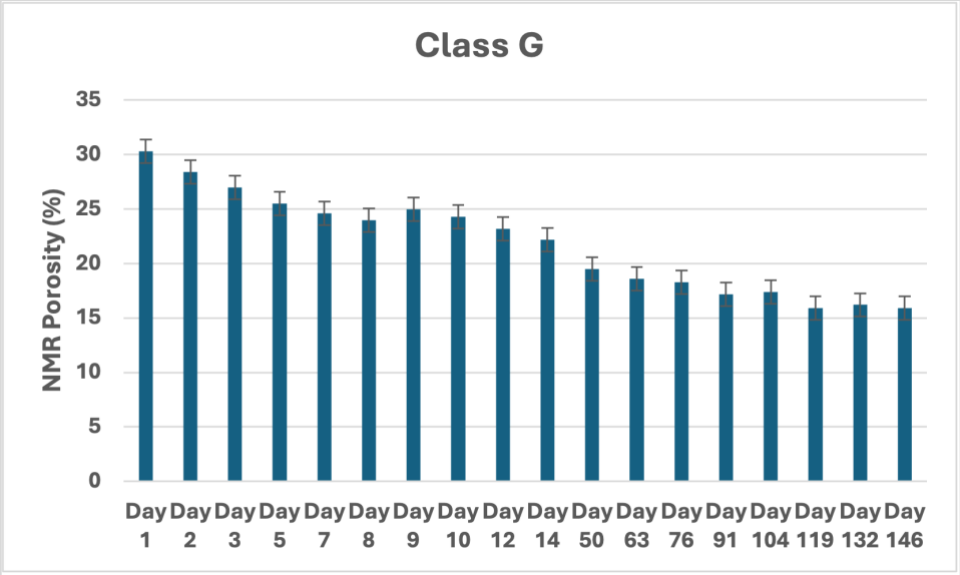

Figure 15: NMR Porosity for Class G Cement: Day-by-Day Measurement Over 146 Days

4.2 Class G + 5% Microblock

Figures 16 and 17 display the NMR porosity behavior of Class G cement with 5% Microblock (MB) additive, cured under room temperature conditions over 146 days. Initially, the porosity was around 29.5% on day 1, experiencing a sharp decline to approximately 20% by day 10. After this rapid early reduction, the porosity continues to decrease more gradually, stabilizing around 16.9% by day 91 and remaining relatively constant, with the final porosity recorded at 16.2% on day 146. This trend, observed in plots, highlights the role of the Microblock additive in significantly reducing porosity during the early hydration stages and maintaining a stable, low porosity as the cement matrix matures, thereby contributing to the improved density and durability of the cement over time.

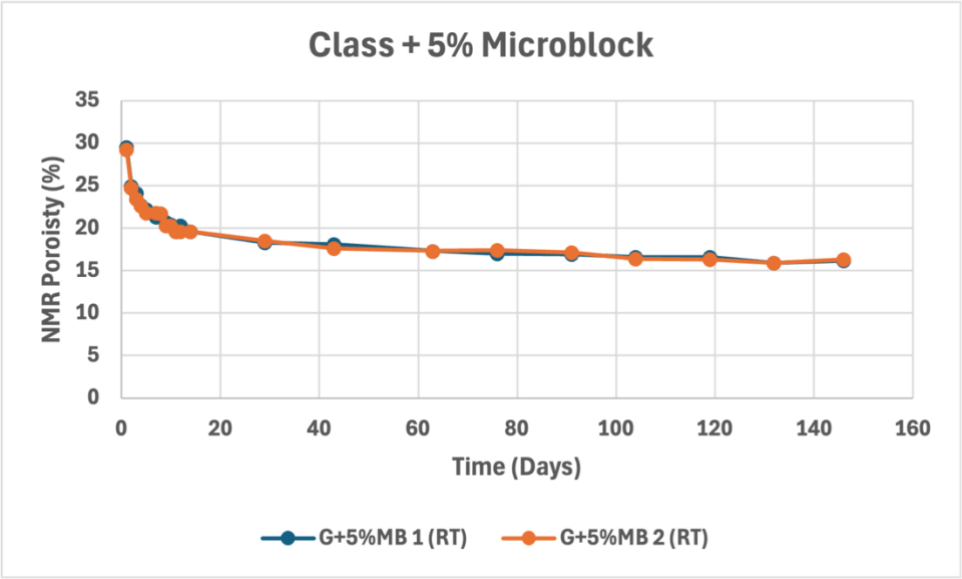

Figure 16: NMR Porosity Over Time for Class G Cement with 5% Microblock at Room Temperature (RT)

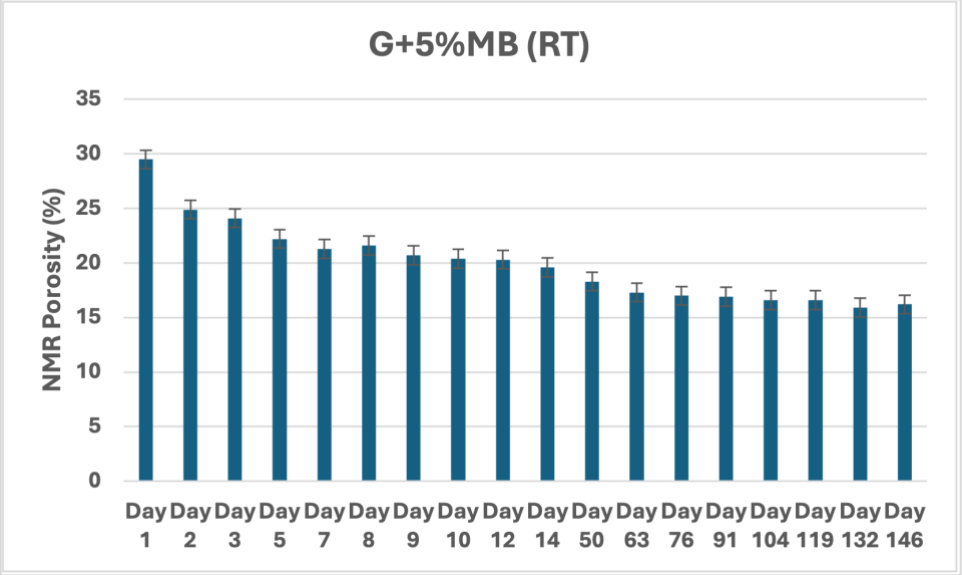

Figure 17: NMR Porosity for G Cement with 5% Microblock: Day-by-Day Measurement Over 146 Days

4.3 Class G + 10% Silica Flour

The results for Class G cement with 10% silica flour (SF) cured at room temperature (**Figures 18 and 19**) show a significant decrease in porosity from 29.4% on day 1 to 22.7% by day 5, followed by a progressive decline over time. By day 50, the porosity drops to 18.0%, and by day 146, it has stabilized at 15.6%. The trend shows an initial quick reduction in porosity during early hydration, followed by a sustained decline, also demonstrating that silica flour is effective at lowering porosity and contributing to the densification of the cement matrix.

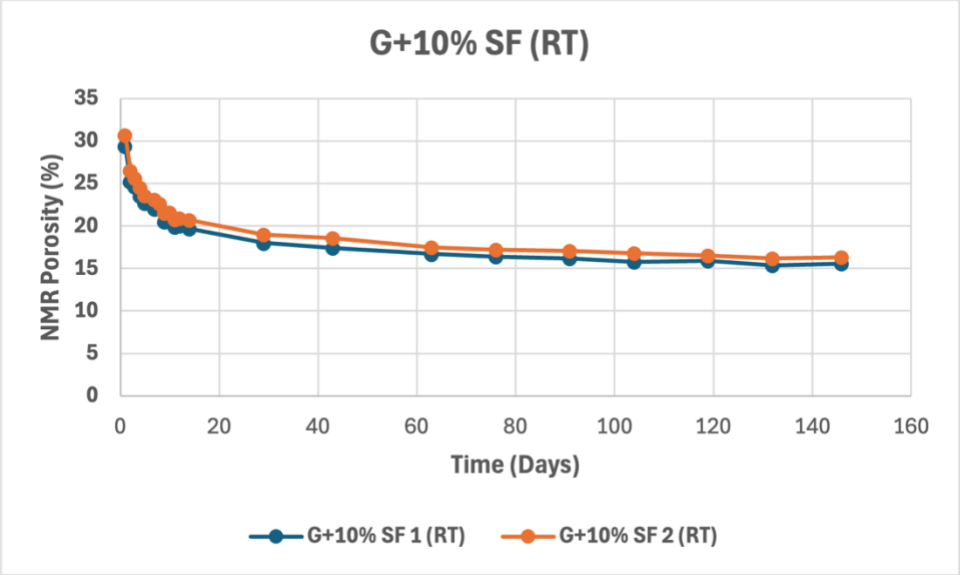

Figure 18: NMR Porosity Over Time for Class G Cement with 10% Silica flour at Room Temperature (RT)

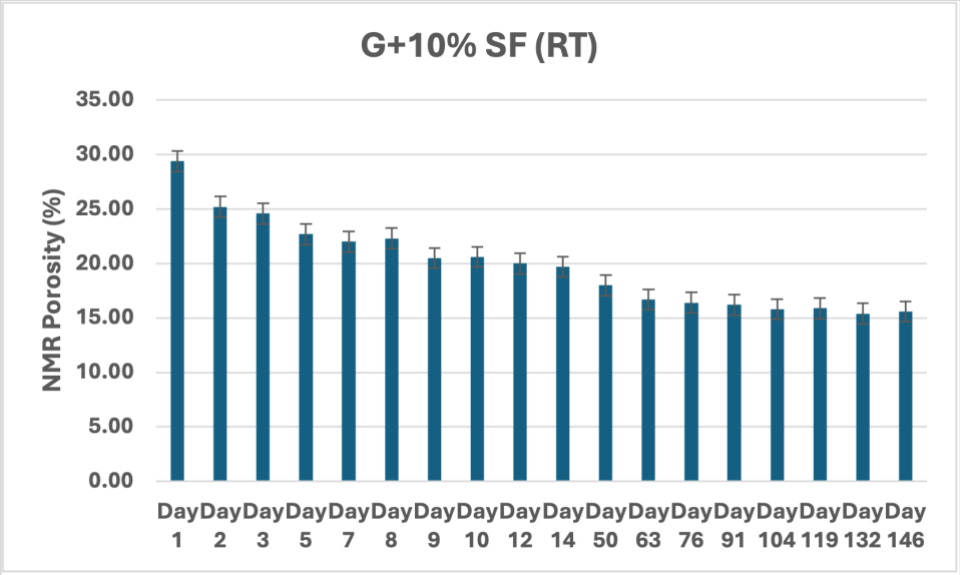

Figure 19: NMR Porosity for G Cement with 10% Silica flour: Day-by-Day Measurement Over 146 Days

4.4 Class G + 5% Micro Cellulose

Similar to class the previous sample, **Figures 20** and **21** show that the NMR porosity results for Class G cement with 5% microcellulose (MC) show a consistent decrease in porosity over time. On day 1, the porosity starts at 29.1%, and by day 10, it drops to 22.9%, indicating that a significant amount of hydration and pore filling occurs in the first few days. After day 10, the reduction in porosity slows down, stabilizing around 17% between days 50 and 104. By day 146, the porosity levels off at 16.1%, indicating that most of the hydration process has been completed, leading to a more compact and stable cement matrix.

The consistent trend observed in both plots reflects the effectiveness of microcellulose in aiding the early densification of the cement, with further gradual improvements in the cement structure over time. The minimal changes in porosity after day 50 suggest that the cement has reached a stable and durable state.

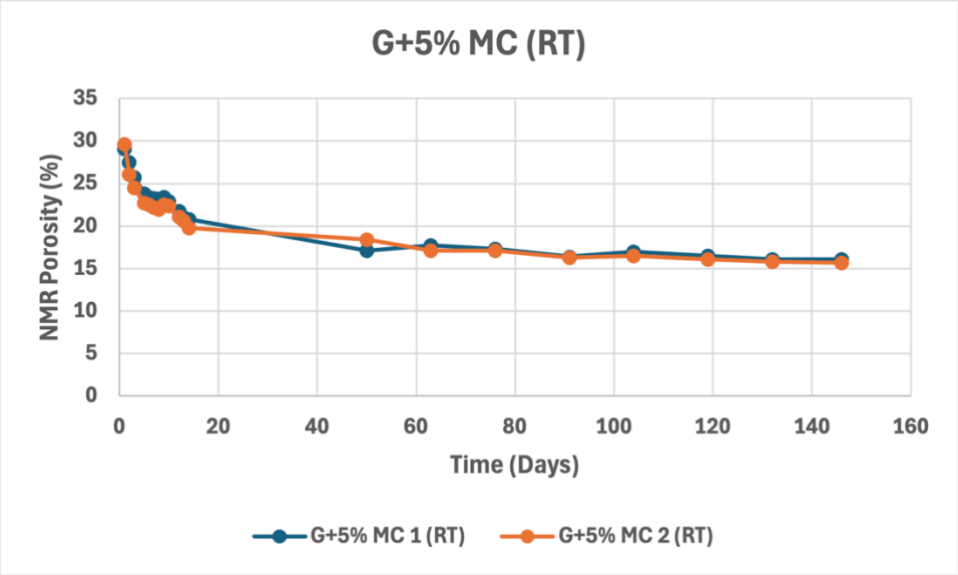

Figure 20: NMR Porosity Over Time for Class G Cement with 5% Micro Cellulose at Room Temperature (RT)

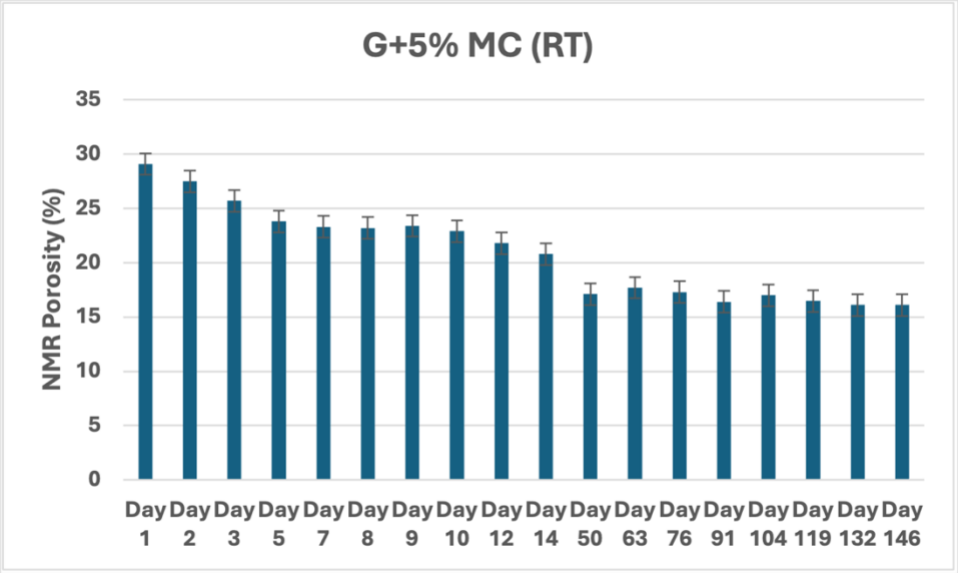

Figure 21: NMR Porosity for G Cement with 5% Micro Cellulose: Day-by-Day Measurement Over 146 Days

4.5 Class G + 10% Fly Ash

The NMR porosity results for Class G cement with 10% fly ash (FA) reveal a clear reduction in porosity over time as shown in **Figures 22** and **23**. Starting at 20.2% on day 1, the porosity decreases by approximately 20% to 16.1% by day 10. By day 50, porosity drops further to 13.1%, marking a total reduction of 35% from the initial value. By day 146, the porosity stabilizes around 10.7%, representing a total decrease of 47% from day 1. This steady reduction, particularly in the early hydration stages, demonstrates the effectiveness of fly ash.

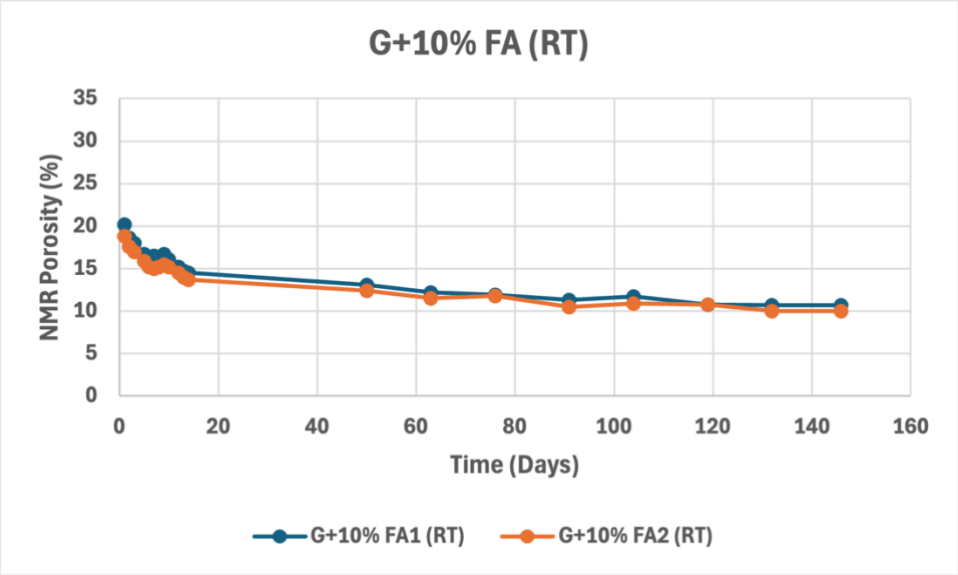

Figure 22: NMR Porosity Over Time for Class G Cement with 10% Fly Ash at Room Temperature (RT)

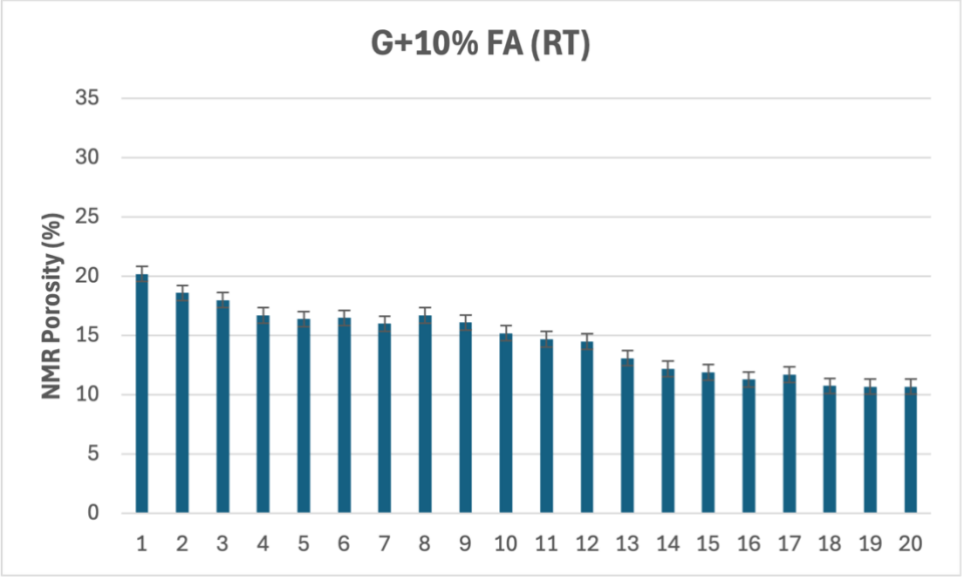

Figure 23: NMR Porosity for G Cement with 10% Fly Ash: Day-by-Day Measurement Over 146 Days

Figure 24 shows the summary of the NMR porosity trends for Class G cement with various additives for 146 days. While all formulations start with porosity values between 20% and 30%, they exhibit a steady decrease over time. Class G with 10% fly ash (FA) stands out, showing the most significant reduction, starting at 20.2% and stabilizing at around 10.7%, indicating greater densification. The other mixes, including those with 5% Microblock (MB), 10% Silica Flour (SF), and 5% Microcellulose (MC), follow similar trends, starting at higher porosity levels (around 29%) and stabilizing around 15-16% by day 146. This comparison result suggests that while all additives help reduce porosity, fly ash is particularly effective in enhancing the cement matrix's density over time.

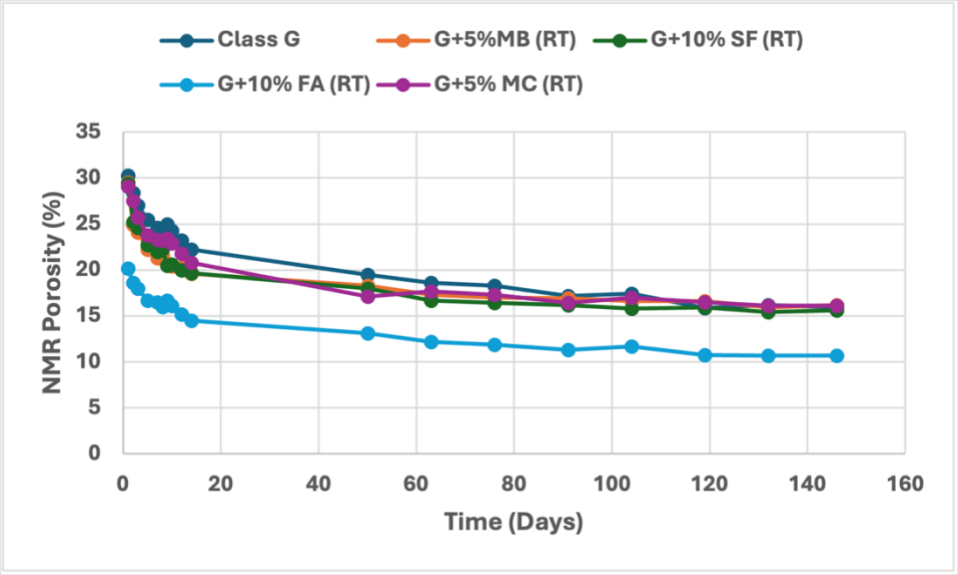

Figure 24: NMR Porosity Trends Over Time for Class G Cement with Various Additives at Room Temperature (RT)

4.6 Class H-neat

NMR porosity measurements for neat class H cement cured under room temperature condition over 146 days indicate a significant reduction in porosity from the initial value of 30.1% to around 12.2% as depicted by **Figure 25** and **26**. This early reduction is likely due to initial hydration reactions and the formation of hydration products, which densify the cement matrix and reduce pore space.

After this initial phase, the rate of porosity reduction slows, stabilizing between days 63 and 146, where porosity fluctuates around 11-12%. This trend suggests that as the cement continues to cure, the ongoing hydration processes contribute to the further densification of the microstructure.

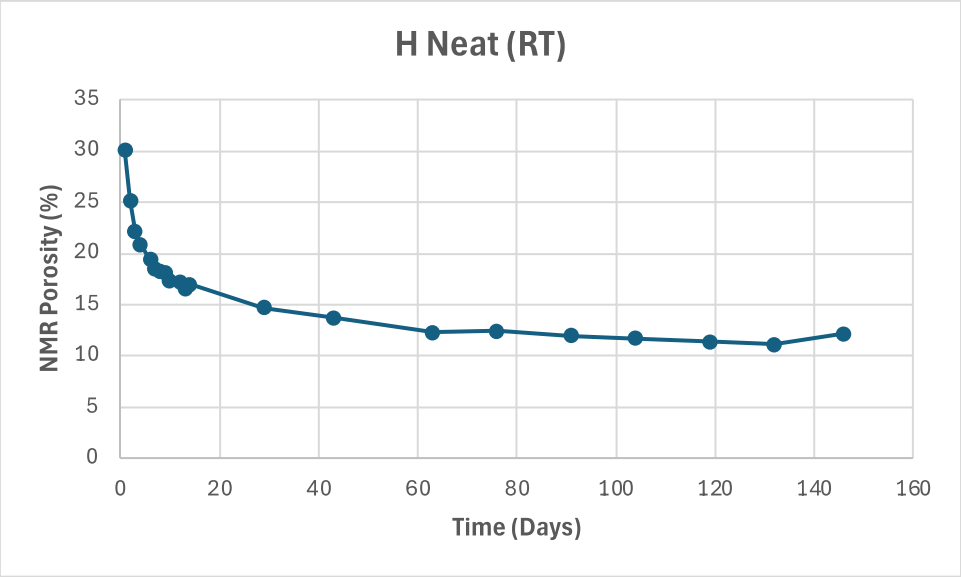

Figure 25: NMR Porosity Over Time for Class H Neat at Room Temperature (RT)

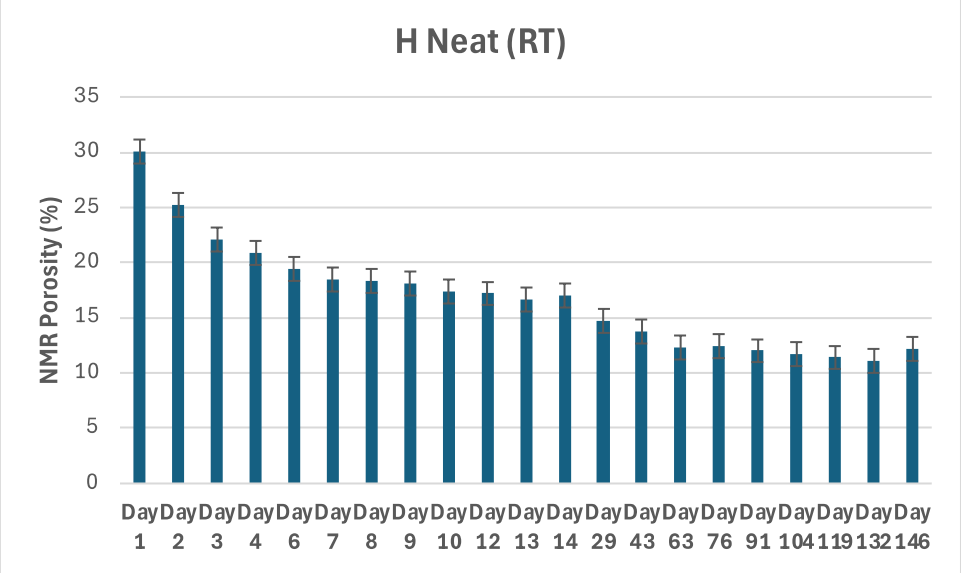

Figure 26: NMR Porosity for H-Neat: Day-by-Day Measurement Over 146 Days

4.7 Class H + 10% FA

The result for class H with 10% fly ash cured under room temperature condition also show consistent reduction in NMR porosity over the 146 days. Starting from an initial NMR porosity of 19.9% on Day 1 to 6.8% by Day 146, this sample shows a steeper decrease in porosity by the end

of the curing period. This trend was also observed for class G with 10% fly ash and is likely due to the hydration of cement and the pozzolanic reactions of fly ash additive, which help fill the pores and densify the cement matrix (**Figures 27** and **28**).

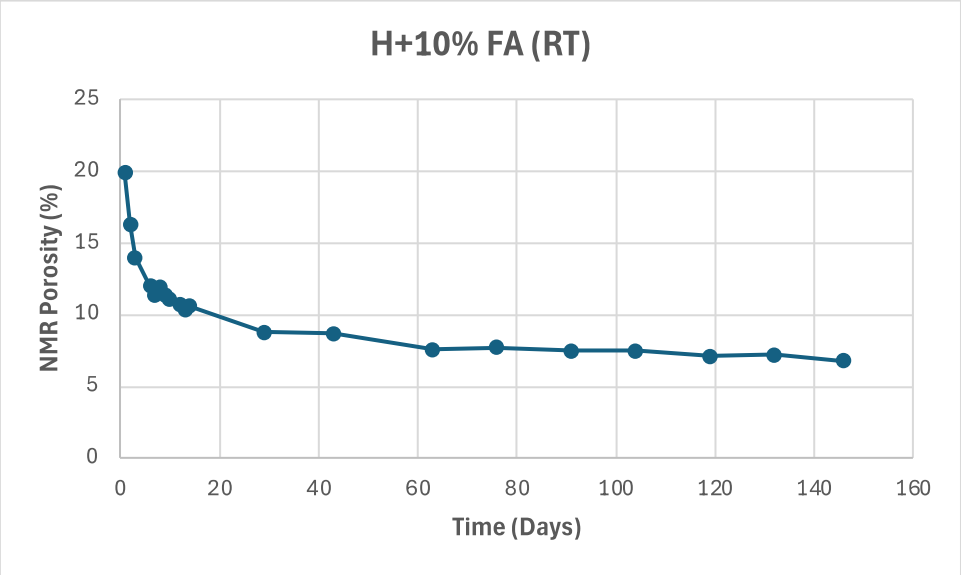

Figure 27: NMR Porosity Over Time for Class H Cement with 10% Fly Ash at Room Temperature (RT)

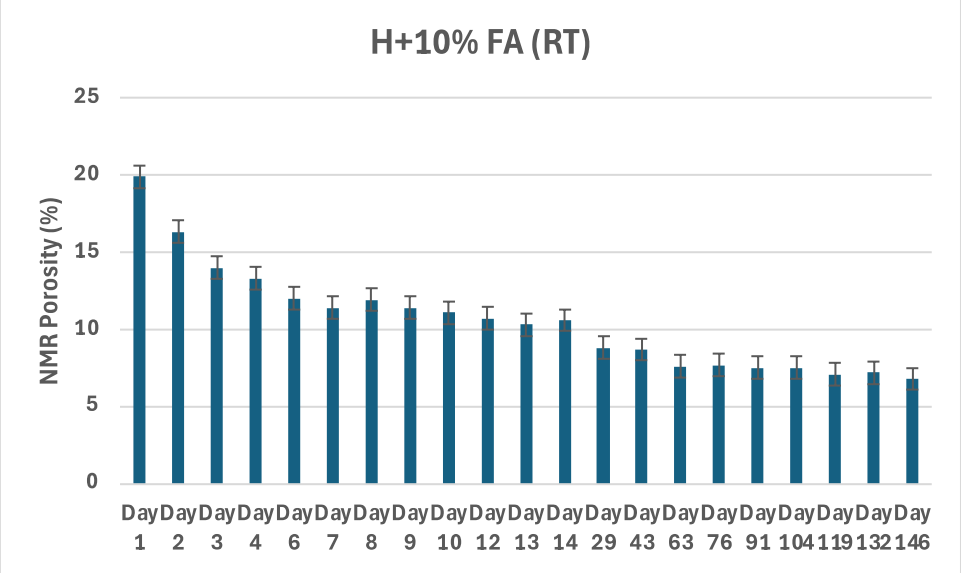

Figure 28: NMR Porosity for H Cement with 10% Fly Ash: Day-by-Day Measurement Over 146 Days

4.8 Geopolymer

The NMR porosity results for the Geopolymer material show minimal variation over time (**Figures 29** and **30**), with porosity values remaining mostly stable between 8.2% and 8.6% during the first 91 days. From day 91 onward, a slight decline in porosity occurs, reaching 7.8% by day 146. This indicates that the geopolymer structure maintains consistent porosity for the majority of the test period, with only minor reductions as curing progresses. The steady porosity values suggest the geopolymer maintains its structure well, with minimal change over time, reflecting its stability compared to other materials.

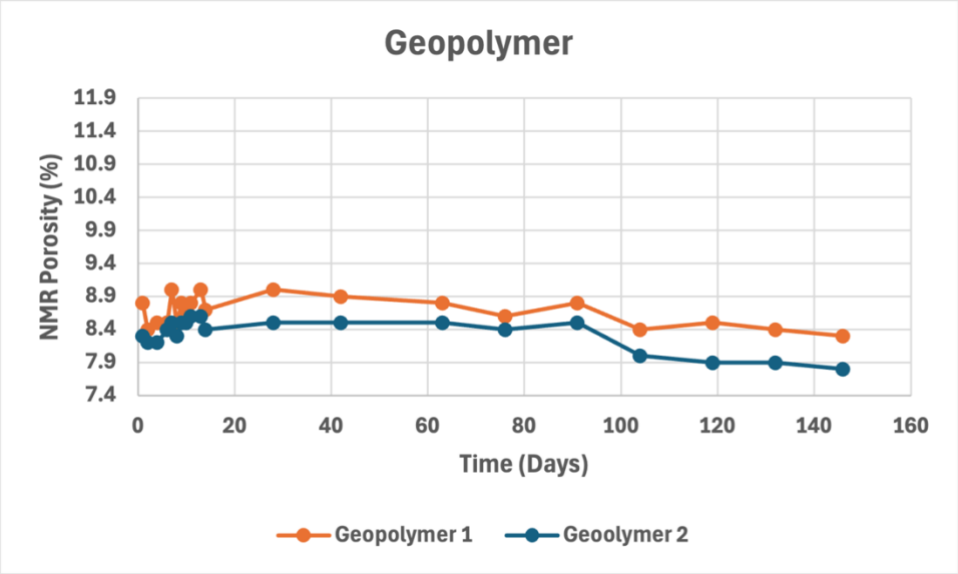

Figure 29: NMR Porosity Over Time Geopolymer cured at 75 degrees Celsius

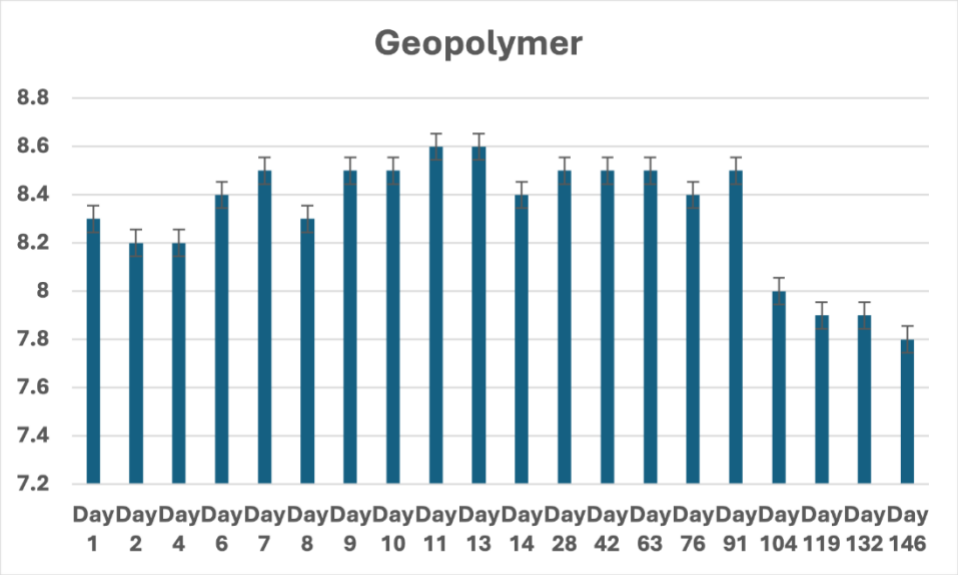

Figure 30: NMR Porosity for Geopolymer: Day-by-Day Measurement Over 146 Days

4.9 High-Temperature Results for G with Fly Ash

Considering the effectiveness of 10% fly ash (FA) in reducing porosity at room temperature, we explored variations of Class G cement with 5%, 10%, and 20% FA at 75°C intending to assess its performance under elevated temperatures.

4.9.1 G+5% FA HT

Figure 31 shows the NMR porosity results for Class G cement with 5% fly ash (FA) at high temperatures (HT) for 35 days. The porosity starts at 17.7% on day 1 and decreases slightly, reaching a minimum of 16.8% by day 11. After this point, the porosity gradually increases, stabilizing around 17.8% by day 35. This indicates an initial reduction in porosity during the early stages of curing.

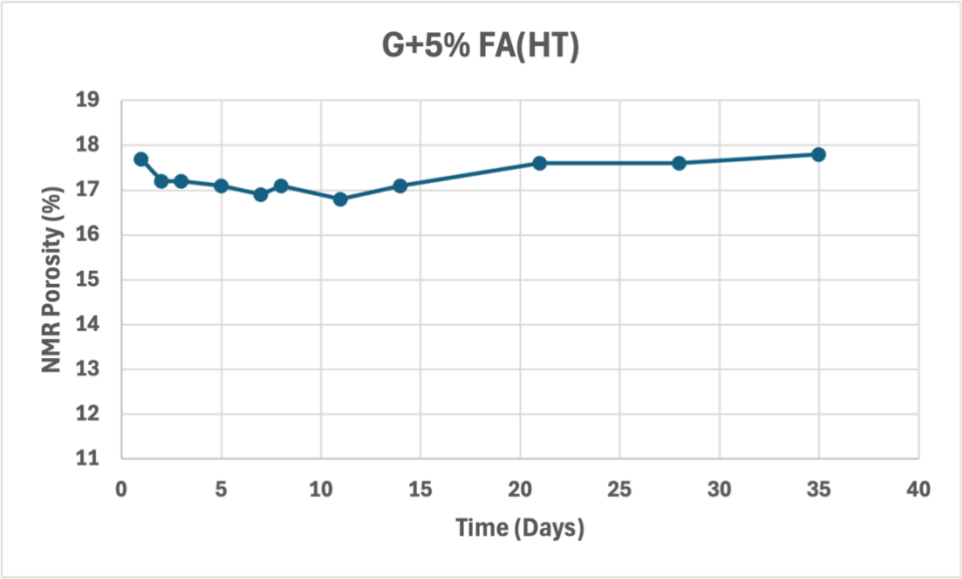

Figure 31: NMR Porosity Trends for Class G Cement with 5% Fly Ash (FA) at High Temperature (HT)

4.9.2 G+10% FA HT

Figure 32 below shows the NMR porosity results for Class G cement with 10% fly ash (FA) at high temperature (HT) showing an initial porosity of 15.3% on day 1. Similarly, over the next 11 days, the porosity fluctuates slightly, reaching a low of 14.5%. After this initial drop, the porosity increases again, peaking at 15.3% by day 21. From there, it slightly declines to 15.1% by day 35. This trend suggests that while there is some initial densification of the material, the porosity stabilizes around the initial values over time under elevated temperatures.

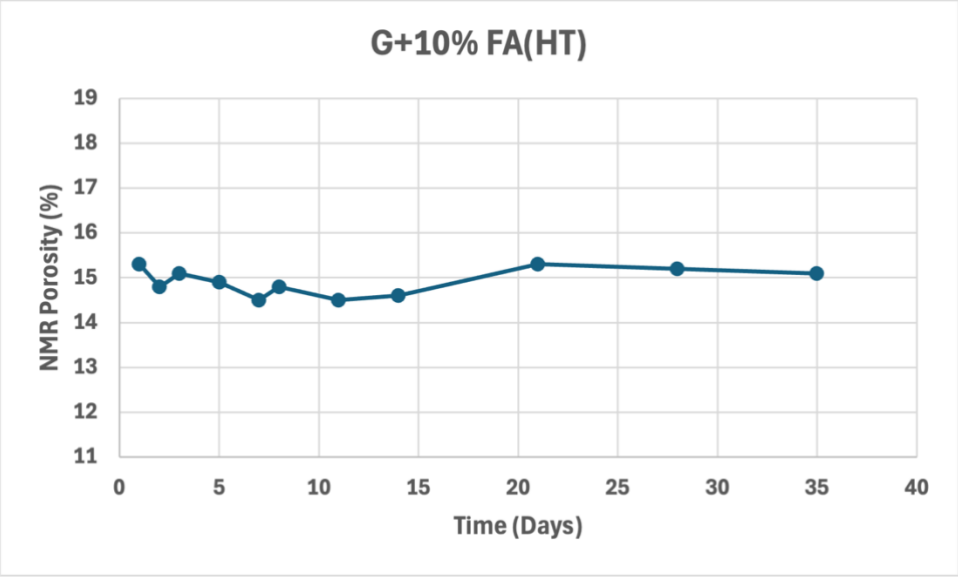

Figure 32: NMR Porosity Trends for Class G Cement with 10% Fly Ash (FA) at High Temperature (HT)

4.9.3 G+20% FA HT

Finally, **Figure 33** depicts the NMR porosity changes for Class G cement with 20% FA over 35 days at high temperatures. The initial porosity of 11.9% on day 1 decreases to 11.1% by day 7, followed by slight fluctuations throughout the testing period. The porosity increases to 11.8% by day 21, stabilizing around 11.7% by day 35. This trend suggests that while some early densification occurs, the porosity remains relatively stable, showing minimal long-term change at elevated temperatures.

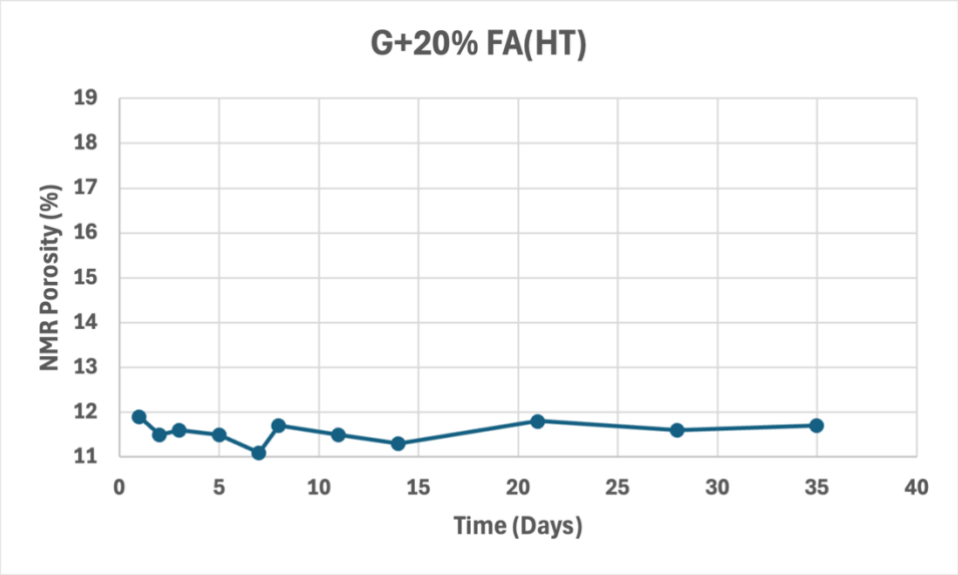

Figure 33: NMR Porosity Trends for Class G Cement with 20% Fly Ash (FA) at High Temperature (HT)

5 Discussions

The discussion chapter will provide a comprehensive analysis of the experimental results, linking them to the objectives of the study. It will explore the long-term NMR porosity of neat class G cement and the impact of various additives (such as fly ash, silica flour, microblock, and microcellulose) on the NMR porosity of Class G cement under room temperature curing conditions. It will analyze the long-term NMR porosity of class H neat cement and the impact of fly ash on class H cement under room temperature curing conditions. The chapter will also examine the influence of elevated temperatures on NMR porosity trends for class G cement with varying fly ash concentrations and geopolymer formulations and how the observed results compare to expectations based on cement hydration.

5.1 Class G vs class G with 10% FA

Comparing the NMR porosity of Class G cement with and without the addition of 10% fly ash (FA) over 146 days at room temperature (**Figure 34**), it is noted that the initial porosity for Class G cement starts at 30.3%, while the porosity for the G+10% FA formulation begins significantly lower at 20.2%. This initial difference demonstrates the immediate effect of fly ash on densifying the cement matrix.

Over time, both formulations show a consistent decline in NMR porosity, but the G+10% FA mixture consistently exhibits a more pronounced reduction. By day 10, Class G porosity drops to 24.3%, whereas the G+10% FA formulation reaches 16.1%. As the curing process progresses, the differences in porosity become more evident. By day 50, Class G porosity is at 19.5%, while G+10% FA falls to 13.1%. This trend continues, with the fly ash mix stabilizing at around 10.7% by day 146, compared to 15.9% for Class G.

The more substantial reduction in NMR porosity for the G+10% FA mixture suggests that fly ash enhances the densification process, potentially due to the pozzolanic reaction where fly ash reacts with calcium hydroxide to form additional calcium silicate hydrates (C-S-H). This reaction improves the cement matrix's density, reducing porosity more effectively than in the Class G formulation without FA.

The reduction in porosity observed in this current study aligns with earlier findings, such as those reported by Thomas (2007) and Bouzoubaa et al., (2001) who found that fly ash, when used as a partial replacement for cement, reacts with calcium hydroxide to form additional calcium silicate hydrates (C-S-H). This pozzolanic reaction contributes to filling the voids in the cement matrix, leading to lower porosity and increased density over time. These findings highlight the effectiveness of fly ash as an additive for reducing porosity, which could translate into improved durability, reduced permeability, and better overall performance of the cement, particularly in applications requiring long-term stability. The consistent and more significant decrease in porosity in the fly ash mix supports the hypothesis that FA significantly improves the microstructural properties of cement over time, even under room temperature conditions.

It is important to note that the reduction in porosity is not a result of shrinkage; this is because the mechanism of hydration involves the consumption of water to form hydration products, such as calcium silicate hydrate (C-S-H) and other crystalline phases like ettringite. These hydration products occupy space within the pore structure, effectively filling and refining the pores rather than causing a volumetric contraction of the cement matrix (Abid et al., 2019; Poppe & De Schutter, 2005; Ye et al., 2007).

Additionally, hydration leads to densification of the cement paste due to the progressive filling of voids by the newly formed hydration products. The decrease in porosity is primarily attributed to

this densification process and the continuous chemical reaction of water with cement, which reduces the volume of unhydrated cement and pore water.

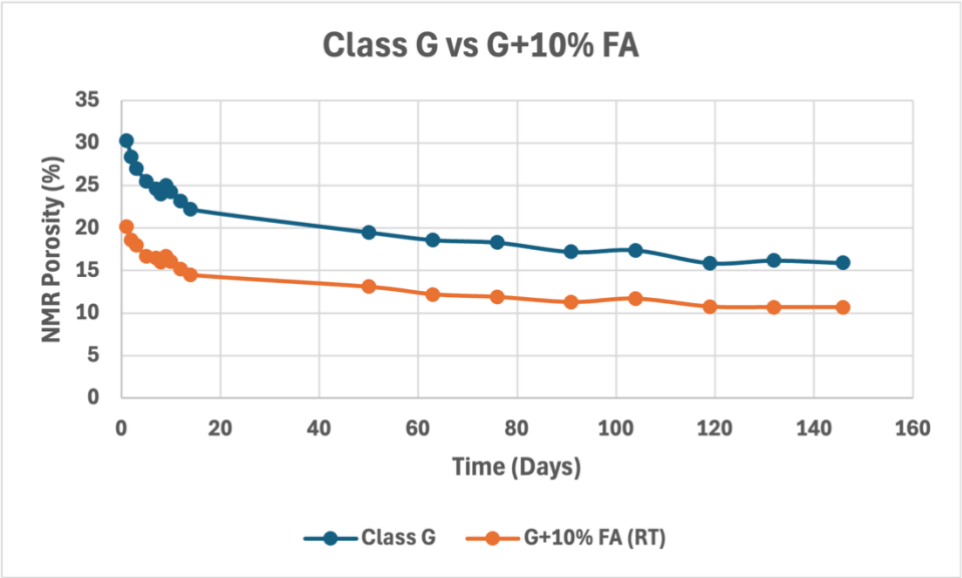

Figure 34: Impact of 10% fly ash on class G cement under room temperature condition

5.2 Class G vs class G with 10% SF

In this comparison between Class G and G+10% Silica Flour (SF) (**Figure 35**), it is observed that the NMR porosity for both also samples decrease over time. G+10% SF exhibits a slightly better performance in reducing porosity across the entire curing period compared to Class G. At the start, Class G has a porosity of 30.3%, while G+10% SF starts at 29.4%, showing only a minor initial difference. However, by day 146, the porosity of G+10% SF drops to 15.6%, compared to Class G's 15.9%. The most noticeable reduction occurs within the first 50 days, where G+10% SF falls from 29.4% to 18.0%, a sharper decline compared to Class G, which moves from 30.3% to 19.5%. This trend suggests that the addition of silica flour has a modest but consistent impact on reducing NMR porosity, making the cement matrix slightly denser over time. This behavior could be attributed to the concentration of silica in the silica flour while it contributes to the refinement of

the pore structure, its addition at 10% does not dramatically outperform the inherent hydration capabilities of Class G neat cement under the studied conditions. A higher dosage, finer silica flour, or elevated curing temperatures might reveal a more distinct impact.

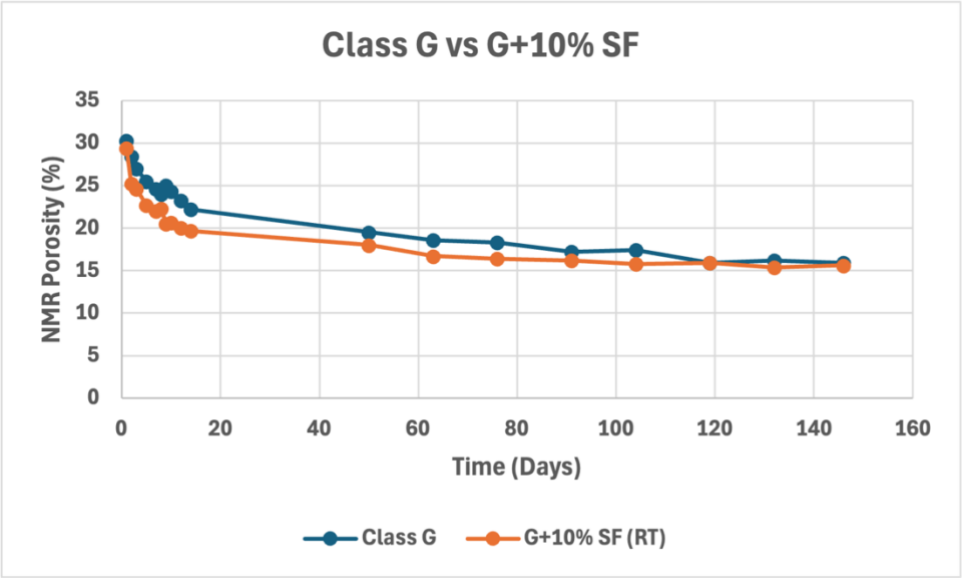

Figure 35: Impact of 10% silica flour on class G cement under room temperature condition

5.3 Class G vs class G with 5% MB

Figure 36 shows the tendency that was observed, with the addition of 5% microblock (MB) which accelerates the reduction in NMR porosity during the early stages of curing, with G+5%MB consistently exhibiting lower NMR porosity than Class G cement within the first 50 days. Specifically, G+5%MB sees a faster drop from 29.5% to 19.6% in the first 14 days, while Class G drops more slowly, from 30.3% to 22.2%.

However, after the initial rapid decline, the rate of NMR porosity reduction for G+5%MB slows down, and the difference between the two formulations narrows. By day 91, both G+5%MB and Class G show similar values, and by day 146, class G slightly outperforms G+5%MB with a final porosity of 15.9% compared to 16.2%. The early acceleration in porosity reduction could be

attributed to the microblock's physical and chemical contributions, but over time, as the hydration process stabilizes and microblock's effects reach saturation, the differences between G+5%MB and Class G become less significant.

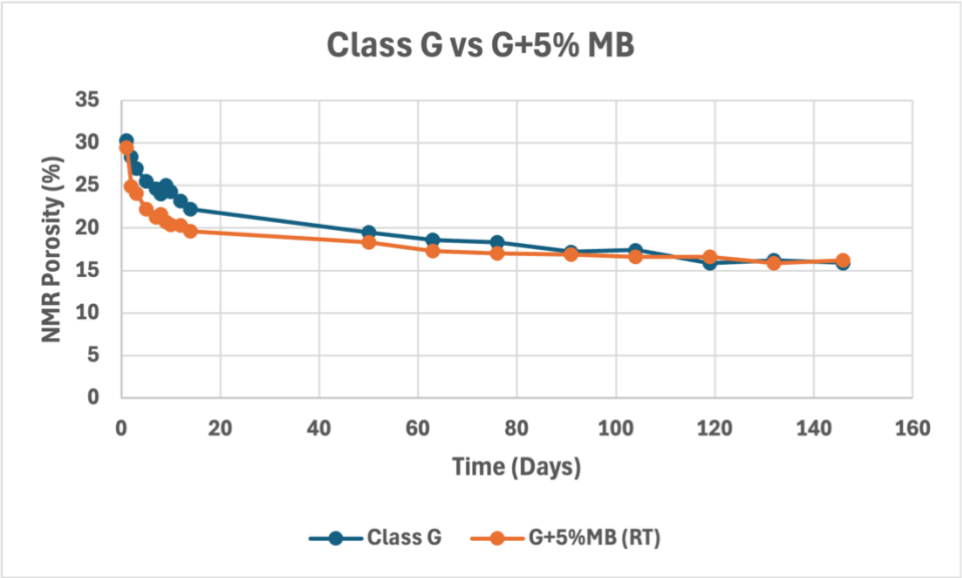

Figure 36: Impact of 5% micro block on class G cement under room temperature condition

5.4 Class G vs class G with 5% MC

For this formulation, the NMR porosity trend follows a similar initial pattern to the other formulations, with a notable reduction in porosity over the first few days. On Day 1, the porosity starts at 29.1%, only slightly lower than the 30.3% for neat Class G. Over the next few days, the porosity drops significantly, reaching 22.9% by Day 10, showing a reduction of approximately 21% as shown in **Figure 37**. This early reduction suggests that Microcellulose effectively aids in reducing pore spaces during the early hydration phases. By Day 50, the porosity decreases further to 17.1%, indicating a total reduction of about 41% from the initial value. At the final measurement on Day 146, the porosity stabilizes at 16.1%, which is slightly higher than class G's final porosity of 15.9%. This could indicate that while Microcellulose aids in reducing porosity initially, its long-

term effect seems to level off, resulting in similar porosity values as the neat class G formulation at the end of the curing period.

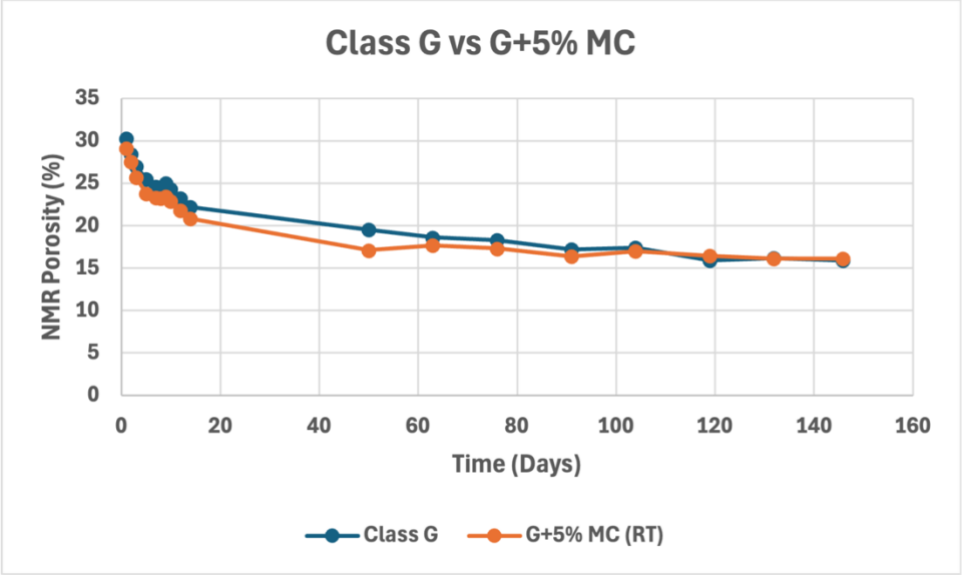

Figure 37: Impact of 5% micro cellulose on class G cement under room temperature condition

Summarily, **Figure 38** shows that all cement formulations with additives show a decrease in NMR porosity over time. G+10% Fly Ash (FA) consistently exhibits the lowest porosity, indicating it is the most effective additive for reducing porosity. Other additives, such as Microcellulose (MC), Microblock (MB), and Silica Flour (SF), also show improvements at the early stages of hydration, their porosity levels stabilize around 16% by Day 146, slightly higher than G+10% FA. This suggests that while all additives enhance cement densification, fly ash provides the most significant long-term reduction in porosity.

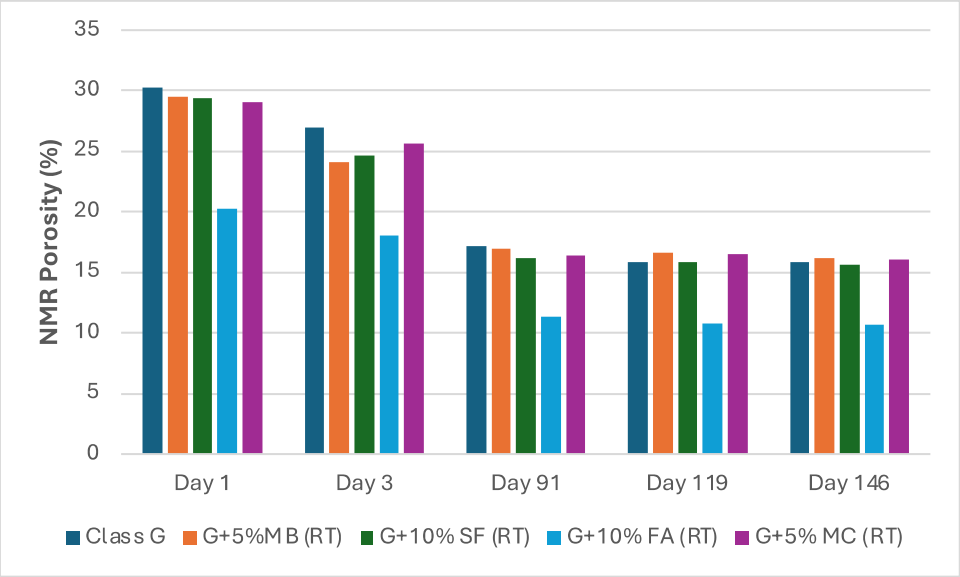

Figure 38: Comparison of NMR porosity of Class G cement with different additives (5% Microblock (MB), 10% Silica Flour (SF), 10% Fly Ash (FA), and 5% Microcellulose (MC)) at selected days

5.5 Class G + FA variations

The NMR porosity trend for G+5% fly ash under room temperature (RT) and high temperature (HT) conditions demonstrates distinct behaviors over 35 days (**Figure 39**). At room temperature, there is a continuous decline in porosity from 22.3% to 13.7%, indicating a significant densification and reduction in pore spaces over time. In contrast, the high-temperature condition shows a more stable porosity, starting at 17.7% and slightly increasing to 17.8% by day 35. The higher initial NMR porosity reduction at room temperature suggests more effective pore-filling and densification processes. In contrast, the limited changes under HT conditions may be attributed to accelerated early hydration, resulting in a more stable pore structure that exhibits fewer changes over the subsequent days.

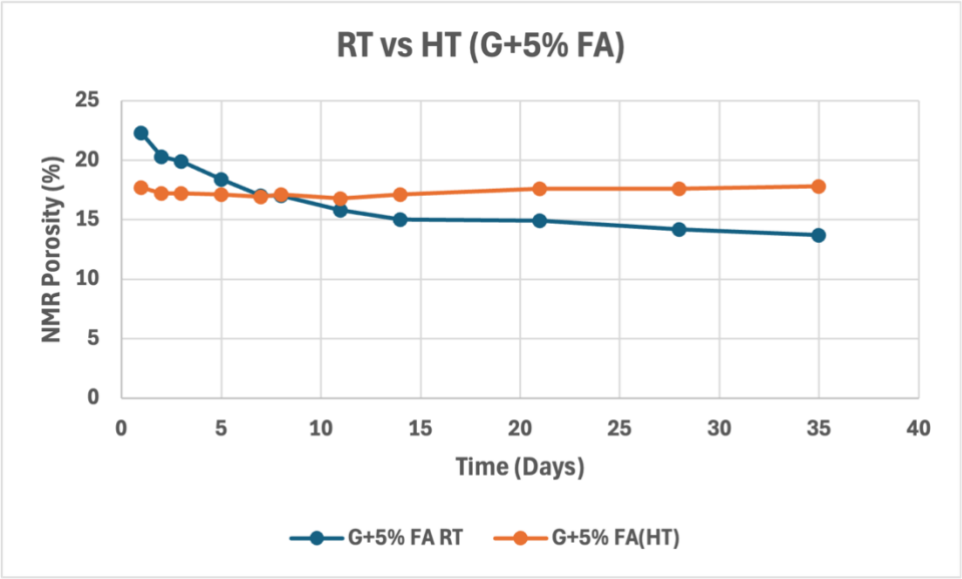

Figure 39: NMR Porosity Trends for G+5% Fly Ash Under Room and High Temperature Conditions

The plot (**Figure 40**) shows the NMR porosity trends for G+10% fly ash (FA) under room temperature (RT) and high temperature (HT) conditions over 35 days. Initially, the room temperature sample starts with a higher porosity of 18.8%, while the elevated temperature sample begins at 15.3%. As time progresses and hydration. continues, the room temperature sample exhibits a steady decline in porosity, reaching approximately 12.9% by day 35. Conversely, the HT sample remains relatively stable, with minor fluctuations around 14.5% to 15.3% throughout the period.

When comparing this plot to the previous one for G+5% FA, a similar trend is observed where the room temperature samples show a more significant reduction in porosity over time compared to the high temperature sample. However, the initial and final porosity values for G+10% FA at room temperature are lower than those for G+5% FA at room temperature, suggesting that a higher fly ash content (10%) may promote a more significant reduction in porosity at room temperature. In contrast, the elevated conditions seem to stabilize porosity at a higher level, regardless of the fly

ash content, potentially indicating that the benefits of fly ash addition are less pronounced at elevated temperatures. This could be due to the accelerated hydration reactions under high temperature conditions, limiting the further densification that occurs over time. At elevated temperature conditions, it is observed that the samples achieved an approximately stable porosity values within the first 24 hours of hydration.

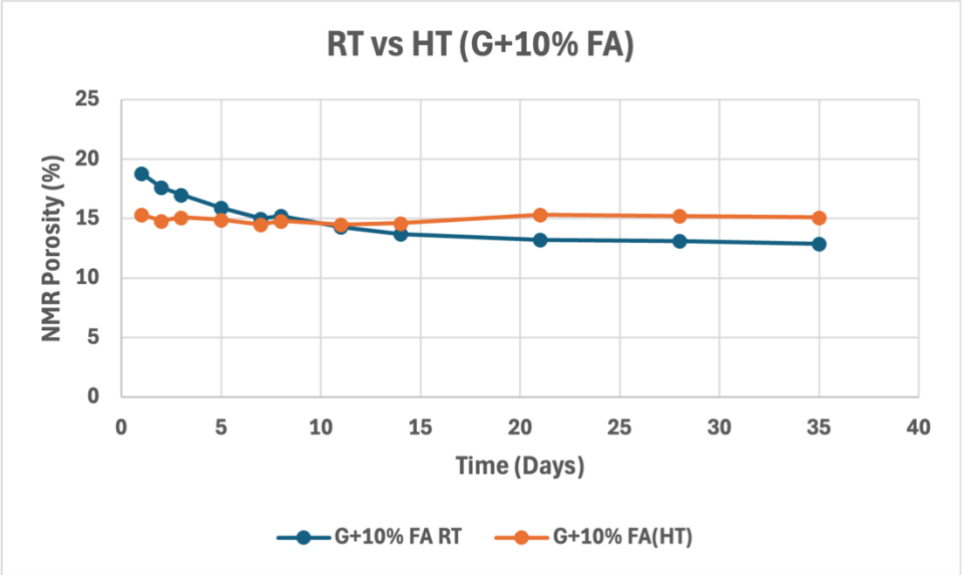

Figure 40: NMR Porosity Trends for G+10% Fly Ash Under Room and High Temperature Conditions

The plot for G+20% FA under both room temperature and high temperature curing conditions shows distinct trends depicted in **Figure 41** below. The room temperature condition initially starts at 15.3% NMR porosity on Day 1 and gradually decreases, reaching 8.9% by Day 35. In comparison, the HT condition starts lower at 11.9%, reflecting a denser matrix early on, but shows a slight increase and fluctuations over time, ending at 11.7%. This pattern suggests that while the room temperature condition continuously reduces porosity, indicating progressive hydration and densification, the high temperature condition stabilizes with minimal change, possibly due to accelerated early hydration that leads to quicker pore structure formation but limited subsequent

densification. Compared to previous observations for lower fly ash content (5% and 10%), the trend confirms that higher fly ash concentration under high temperature conditions achieves early densification and approximately stable NMR porosity values which is achieved within the first 24 hours of curing. The trend also suggests that under high temperature curing condition, there is a correlation between the concentration of fly ash and the NMR porosity value achieved. As the concentration increased, there is a positive implication on the porosity.

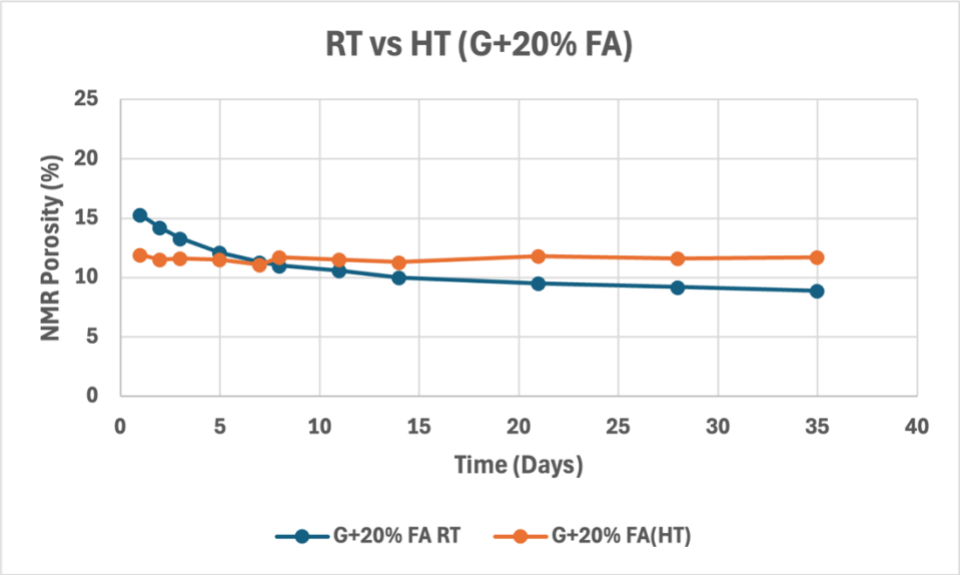

Figure 41: NMR Porosity Trends for G+20% Fly Ash Under Room and High Temperature Conditions

Figures 42 to **45** show a clearer picture of the trends when comparing the two curing conditions, the observed trends indicate that the porosity of the cement samples decreases more significantly when fly ash is added at room temperature (RT) conditions compared to high-temperature (HT) conditions. As seen in **Figures 44** and **45** for RT, the amount of fly ash added is correlated with a steeper reduction in NMR porosity over time, particularly evident from day 1 to day 35. This could mean that a higher fly ash content promotes more effective pore refinement and densification in the cement matrix at room temperature.

On the other hand, the high temperature plots (42 and 43) show that while porosity reduction occurs, it is less pronounced than in the room temperature cases. This can be attributed to the different hydration and pozzolanic reaction rates at elevated temperatures, which may affect the development of the microstructure. Additionally, we observe a tendency for higher initial porosities, which remain relatively stable throughout the days compared to the room temperature results. This stability indicates that while the fly ash addition improves the microstructure, the temperature may moderate the extent of porosity reduction.

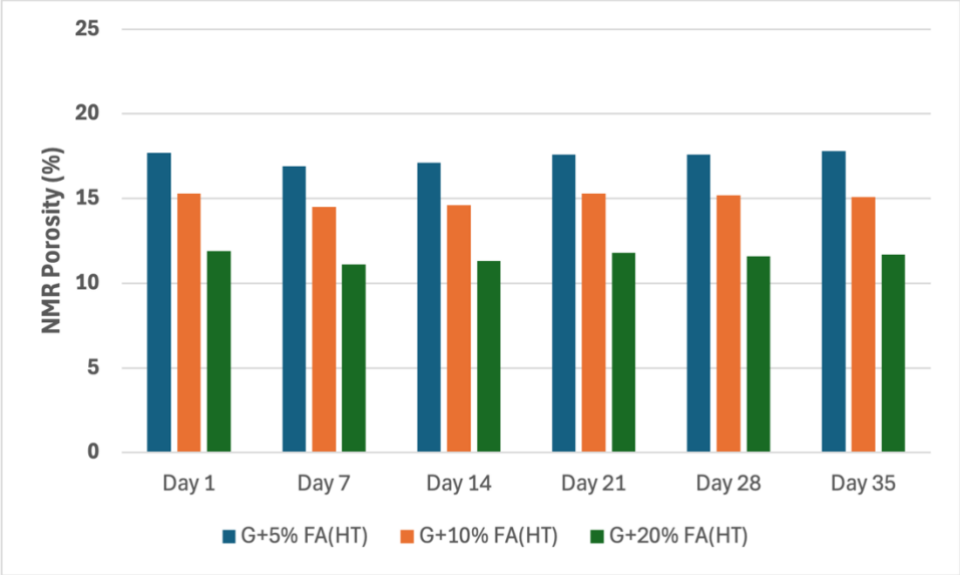

Figure 42: Comparison of NMR porosity of Class G cement with varying percent of fly ash at high temperature for 35 days duration (grouped by days)

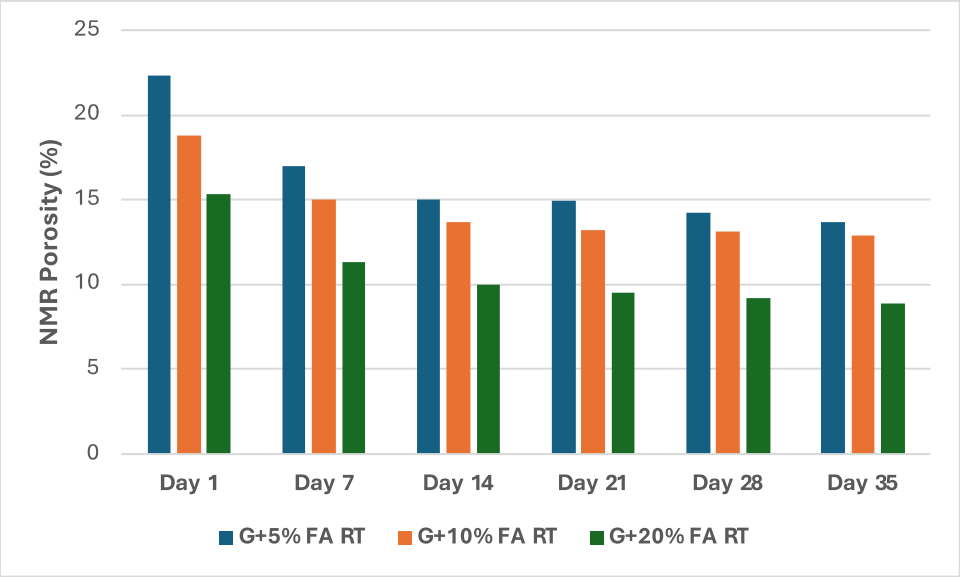

Figure 43: Comparison of NMR porosity of Class G cement with varying percent of fly ash at room temperature for 35 days duration (grouped by days)

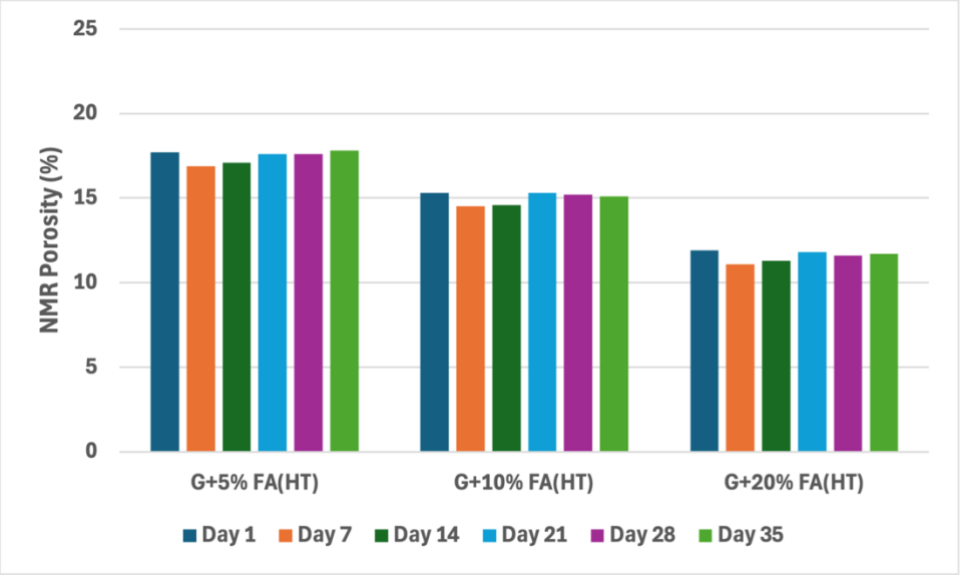

Figure 44: Comparison of NMR porosity of Class G cement with varying percent of fly ash at high temperature for 35 days duration (grouped by additive percentage)

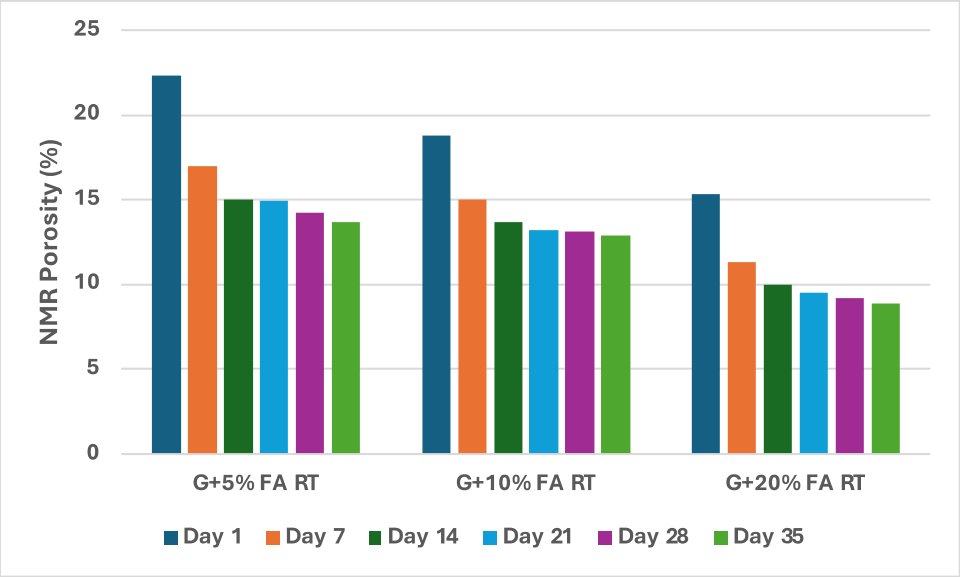

Figure 45: Comparison of NMR porosity of Class G cement with varying percent of fly ash at room temperature for 35 days duration (grouped by additive percentage)

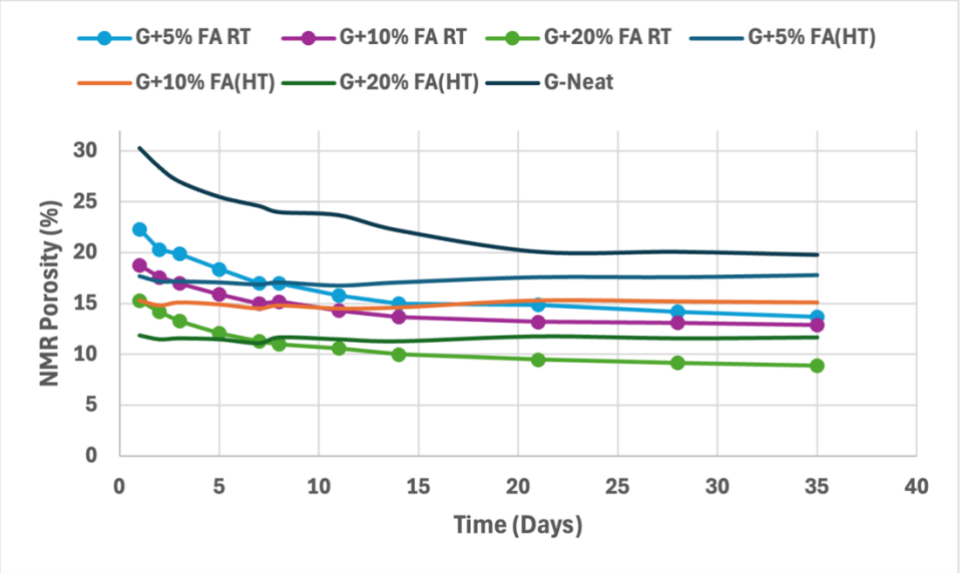

Figure 46: Summary of cement recipes with different percentages of fly ash under both room temperature and high temperature

Figure 46 above summarizes the NMR porosity trends for cement samples with different percentages of fly ash (FA) under both room temperature and high temperature curing conditions over 35 days. In room temperature conditions, all samples show a downward trend in porosity,

with G+20% FA achieving the most significant reduction from an initial 15.3% to 8.9% by Day 35, indicating continuous hydration and densification. Conversely, G+5% FA and G+10% FA under high temperature exhibit relatively stable NMR porosity, with slight fluctuations, suggesting early pore structure stabilization. The G+20% FA HT also stabilizes with minor porosity changes, though it starts with a lower initial porosity. This trend suggests that higher fly ash concentrations and elevated temperatures accelerate early hydration and densification but may limit ongoing reductions in NMR porosity due to early structure formation.

5.6 Class H Neat vs Class H+10% FA

The comparison between H Neat and H+10% FA shows significant differences in the NMR porosity reduction over time. Initially, H Neat starts with a porosity of approximately 30%, while the H+10% FA mix starts much lower, around 20%. Over the 146 days, the addition of 10% fly ash led to a more pronounced decrease in porosity compared to the neat sample. By day 146, the H neat sample stabilizes around 12%, whereas the H+10% FA mix reduces to approximately 6.8% as seen in **Figure 47**.

The fly ash addition likely enhances the cement matrix's densification, filling the pore spaces more effectively due to its fine particles and pozzolanic reaction, which contributes to the long-term decrease in porosity. This behavior aligns with the role of fly ash as a supplementary cementitious material, which improves the microstructure by reacting with the calcium hydroxide produced during hydration, forming additional calcium silicate hydrates (C-S-H) that fill the voids. The trend illustrates how fly ash can significantly improve the cement’s durability by reducing its NMR porosity over time compared to the neat formulation.

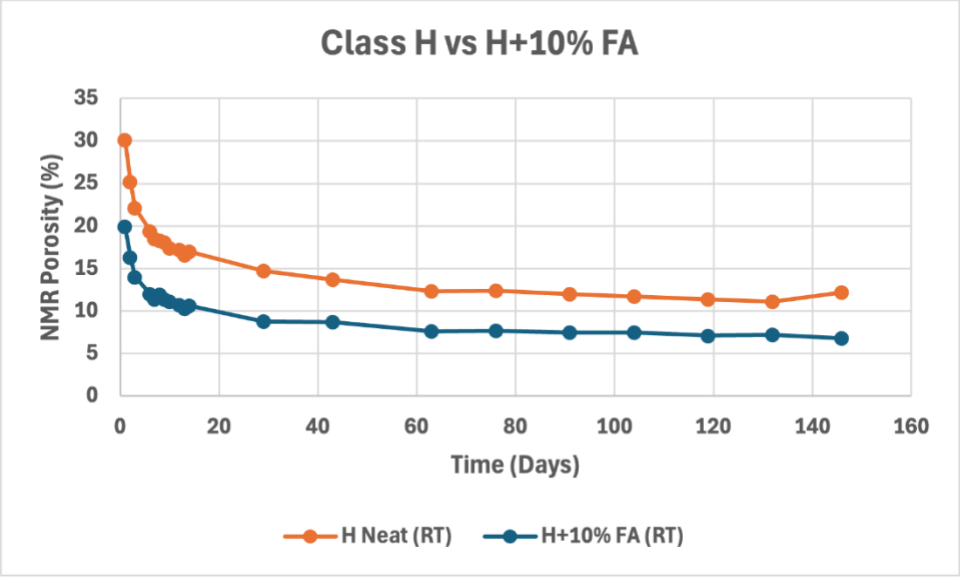

Figure 47: Impact of 10% FA on class H cement under room temperature condition

Similar to the findings of this study, (Ichim, 2017) observed a rapid initial decrease in porosity across at room temperature condition for neat class G with 4% and 12% salt (**Figure 48)**. This initial reduction aligns with the primary hydration reactions in cement, where pore spaces begin to fill as hydration products develop. It was also demonstrated that samples cured at higher temperatures exhibited more variability and generally higher stabilized porosity values which is similar to the high-temperature measurements in this study where fluctuations in the porosity appeared erratic as depicted in **Figure 49**.

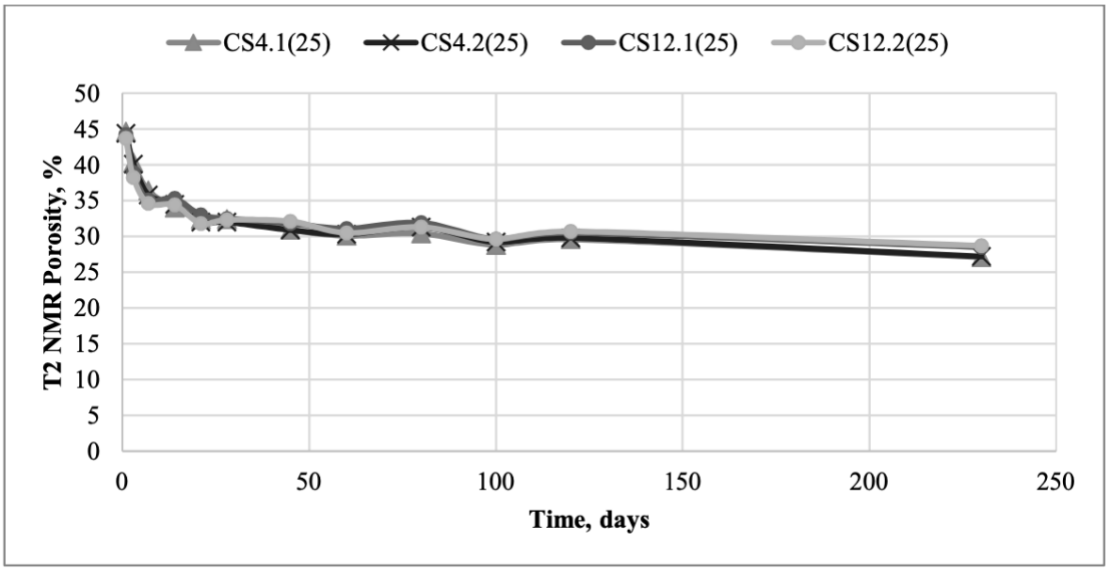

Figure 48: T2 NMR Porosity Evolution for 4% and 12% Salt Cement (25°C) after Ichim (2017)

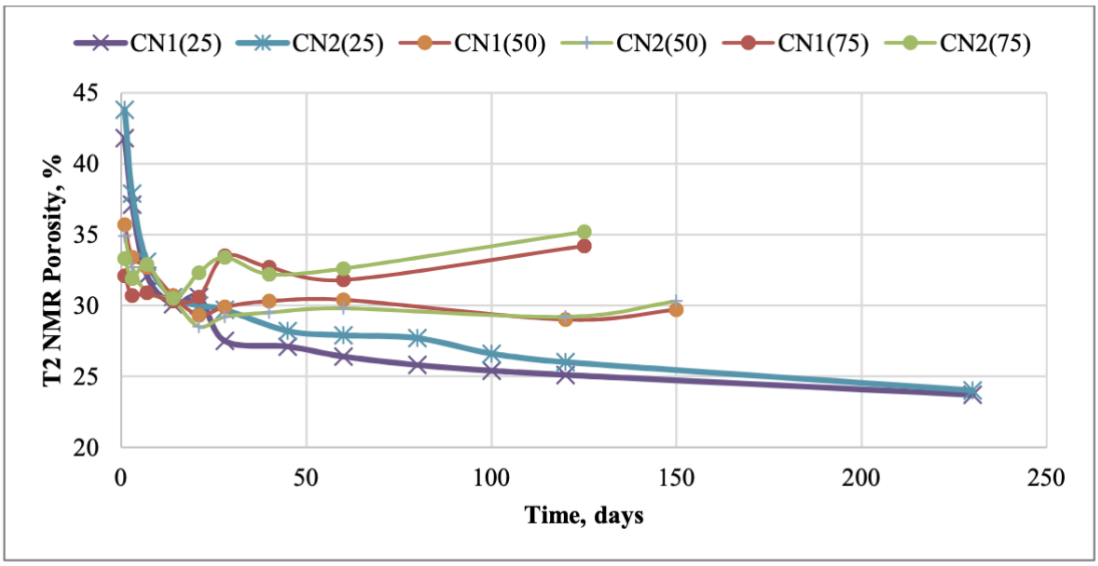

Figure 49: NMR Porosity Evolution in Neat Cement at 25°C, 50°C, and 75°C after Ichim (2017)

5.7 NMR T_2 Distribution Profiles

5.7.1 Room Temperature

The T_2 NMR relaxation time distribution provides insights into the pore structure and water distribution within the cement matrix. In **Figure 50**, the G-neat sample shows the highest peak in the relaxation time range, indicating larger pore sizes or higher water content compared to the samples with various additives. The additives appear to reduce the peak height, suggesting a decrease in pore size or a more refined pore structure.

Among the modified samples, the G+10% SF (Silica Flour) has the most significant shift to the left, indicating the highest degree of pore refinement and reduction in larger pores. G+5% MB (Microblock) and G+5% MC (Microcellulose) also exhibit noticeable shifts, but to a lesser extent than silica flour. G+10% FA (Fly Ash) shows the least shift, suggesting that while it contributes to densification, its impact on pore refinement is less significant compared to silica flour or microblock.

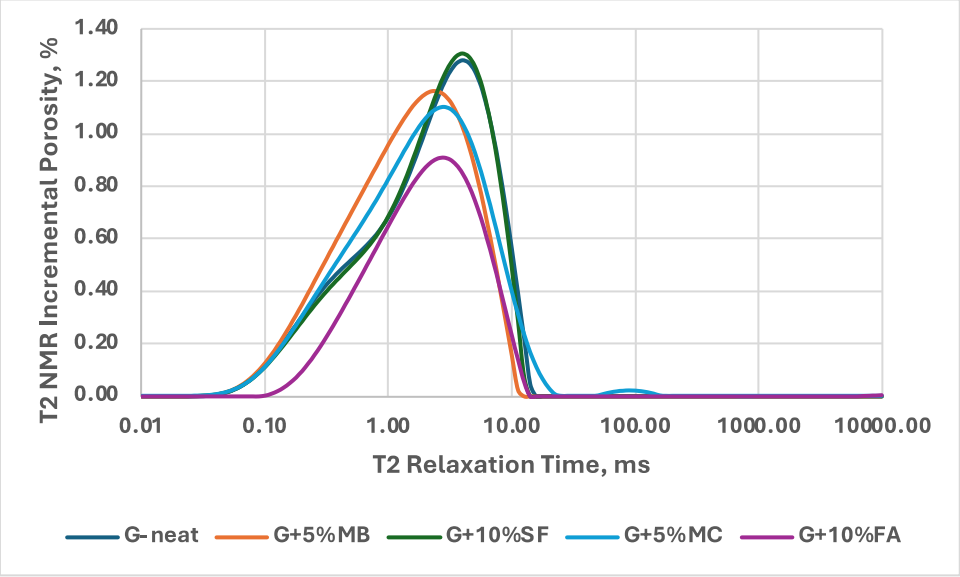

Figure 50: T_2 distribution profile for G-neat, G+5%MB, G+10%SF, G+5%MC, and G+10FA on day 1

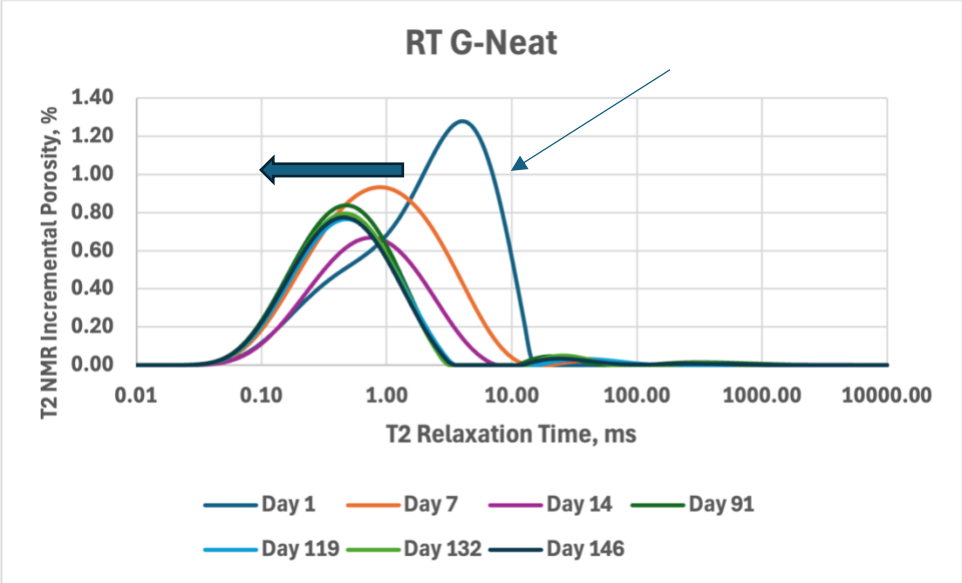

Figure 51: T_2 distribution profile for G-neat cured at room temperature on selected days

The comparison of the pore size distribution for RT G-Neat and RT G+10% FA reveals significant differences in how the cement formulations evolve over time as seen in **Figure 51**. Initially, both formulations exhibit a similar peak position around the 1 ms T_2 relaxation time, indicating comparable pore sizes. However, the RT G-Neat sample shows a more prominent peak on Day 1, suggesting a higher concentration of larger pores compared to the RT G+10% FA sample. Over time, the peak for room temperature G-Neat shifts slightly toward shorter relaxation times, indicating a gradual reduction in pore size and overall porosity. By contrast, the addition of 10% fly ash in RT G+10% Fly ash results in a more stable pore size distribution, with less pronounced shifts in peak positions over time, suggesting that fly ash helps maintain a denser matrix and reduces the coarsening of pores. The overall trend shows that fly ash incorporation stabilizes the microstructure by decreasing the rate of large pore formation and retaining smaller pore sizes even at later stages (Day 146). This indicates that the use of fly ash could be beneficial in enhancing the durability of cement by controlling pore evolution and limiting the development of larger pore spaces over time.

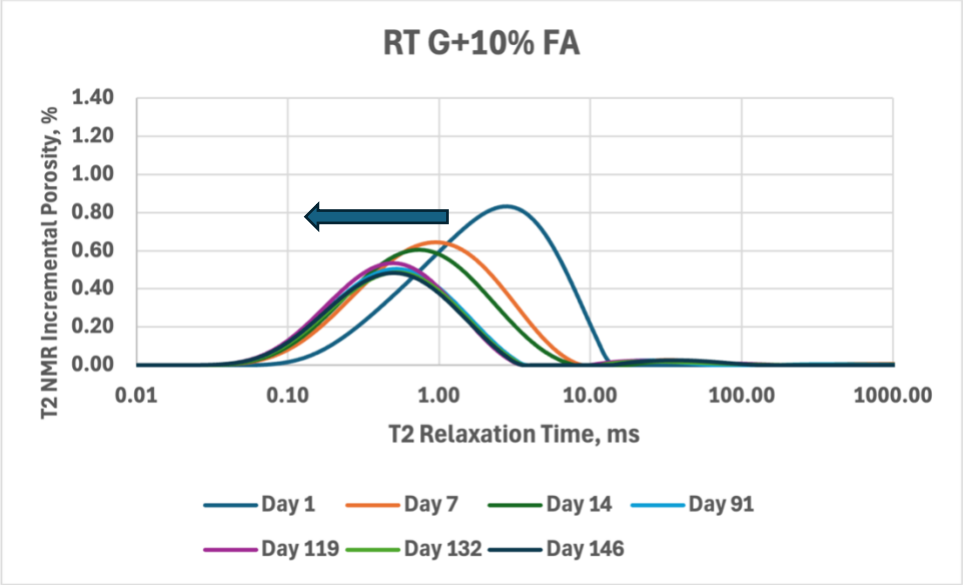

Figure 52: T_2 distribution profile for G+10% FA cured at room temperature conditions on selected days

With the addition of 5% MB (**Figure 53**), the shift in the relaxation time peaks is less pronounced, and the curves are closely clustered. This suggests that the presence of MB may slow the hydration process slightly, stabilizing the pore structure without as much reduction in pore size. For RT G + 10% SF (Silica Flour) (**Figure 54)**, there is a noticeable shift towards shorter relaxation times early in the hydration process (Days 1 to 14), indicating rapid densification. However, beyond Day 14, the shifts plateau, suggesting that the impact of SF on further pore size reduction diminishes over time.

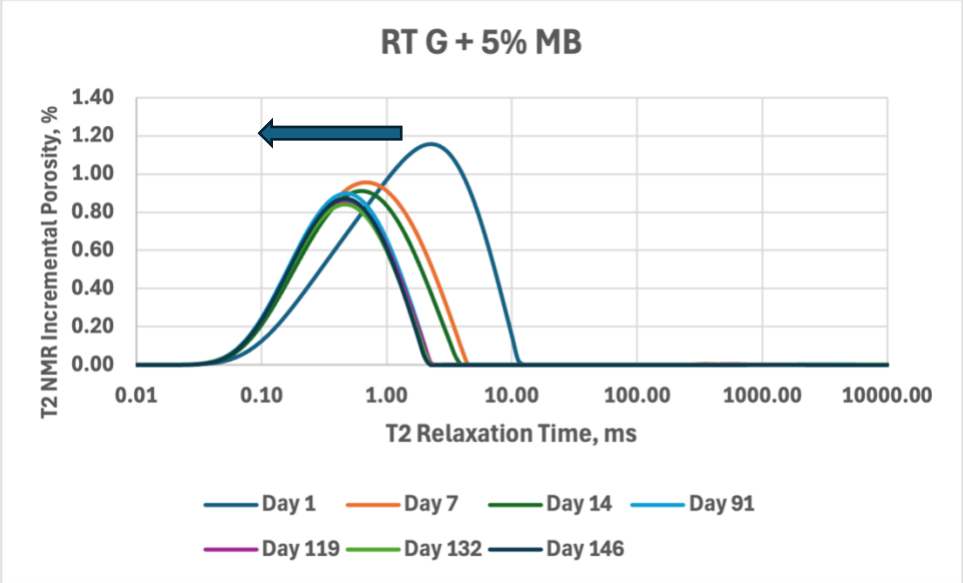

Figure 53: T_2 distribution profile for G+5% MB cured at room temperature conditions on selected days

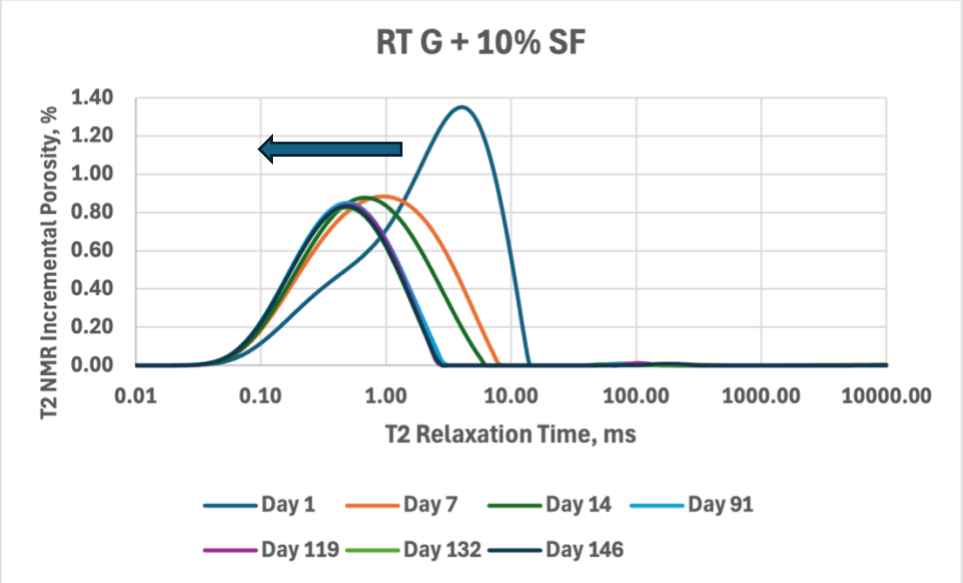

Figure 54: T_2 distribution profile for G+10% SF cured at room temperature conditions on selected days

For the room temperature G + 5% MC sample (**Figure 55**), the shift towards shorter relaxation times is present but less pronounced compared to room temperature G-Neat. The peaks remain

more closely clustered, especially from Day 1 through Day 91, indicating a more stabilized pore structure. This suggests that the addition of Microcellulose may slow down the rate of hydration and pore closure, leading to a more gradual evolution in the microstructure. While there is still evidence of densification, the extent of change in pore size and overall porosity is less dramatic than in the G-Neat sample.

These observations imply that Microcellulose contributes to a slower pace of porosity reduction and may help maintain a more uniform pore structure over time, potentially beneficial for specific cement applications where controlled hydration and sustained microstructural integrity are desired.

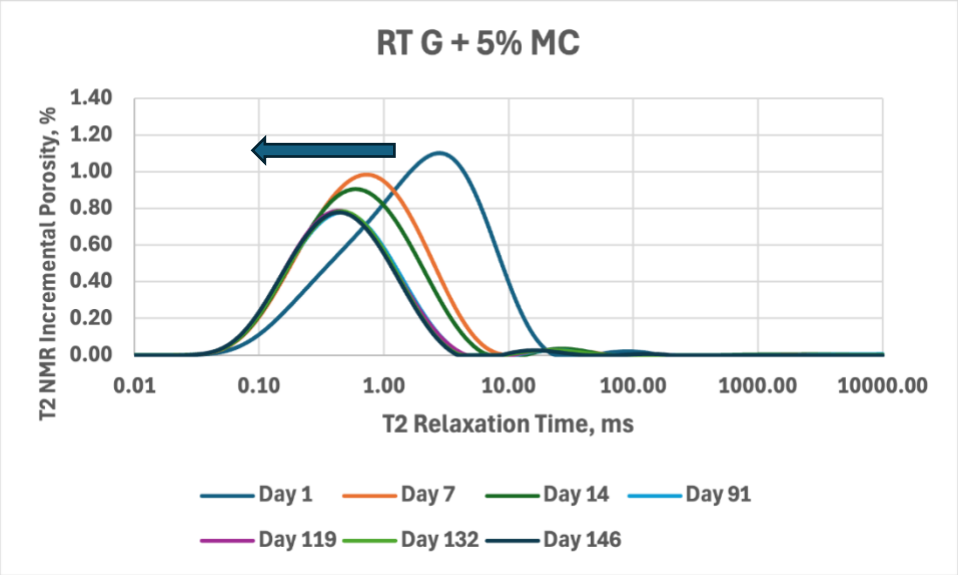

Figure 55: T_2 distribution profile for G+10% MC cured at room temperature conditions on selected days

5.7.2 High Temperature

Comparing the pore size distributions for G+5% FA, G+10% FA, and G+20% FA under high-temperature (HT) conditions reveals some subtle differences. Across all fly ash concentrations, the T_2 relaxation peaks remain relatively stable over time, indicating a consistent pore size distribution. The G+5% FA shows a higher initial peak, suggesting a slightly broader pore size distribution

compared to the G+10% and G+20% FA, which exhibit narrower peaks. As the fly ash content increases, the peaks shift slightly toward shorter relaxation times, indicating smaller average pore sizes. This trend reflects the influence of higher fly ash content on refining the pore structure, enhancing densification. Overall, while all samples display similar profiles, the subtle shifts with increasing fly ash content suggest a progressive improvement in pore size distribution and reduction in larger pores as more fly ash is added **Figure 56-58**. The T_2 pore distribution for geopolymer is also presented below (**Figure 59**) and shows relative stability over time following a similar trend observed for the samples cured at elevated temperature.

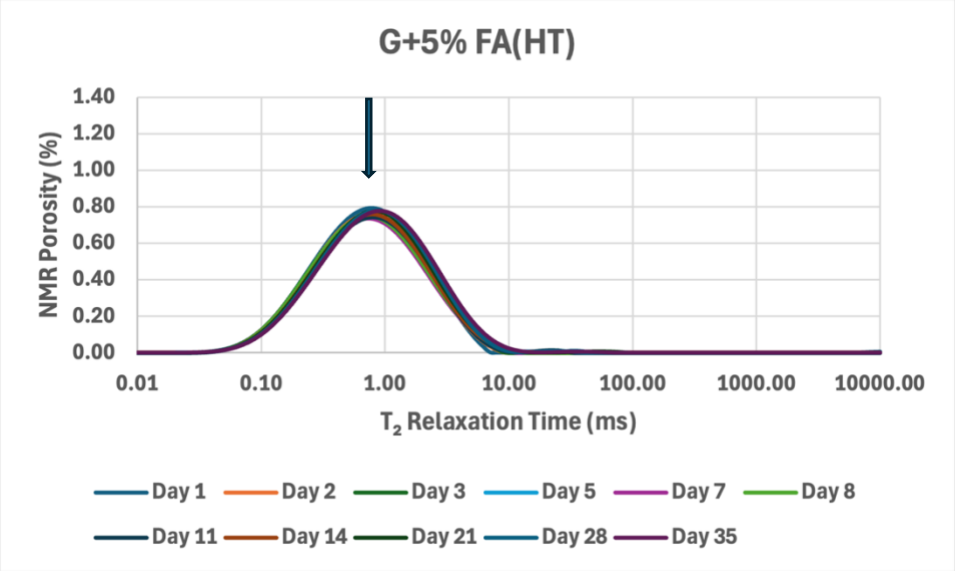

Figure 56: T_2 distribution profile for G+5% FA cured at high-temperature conditions on selected days

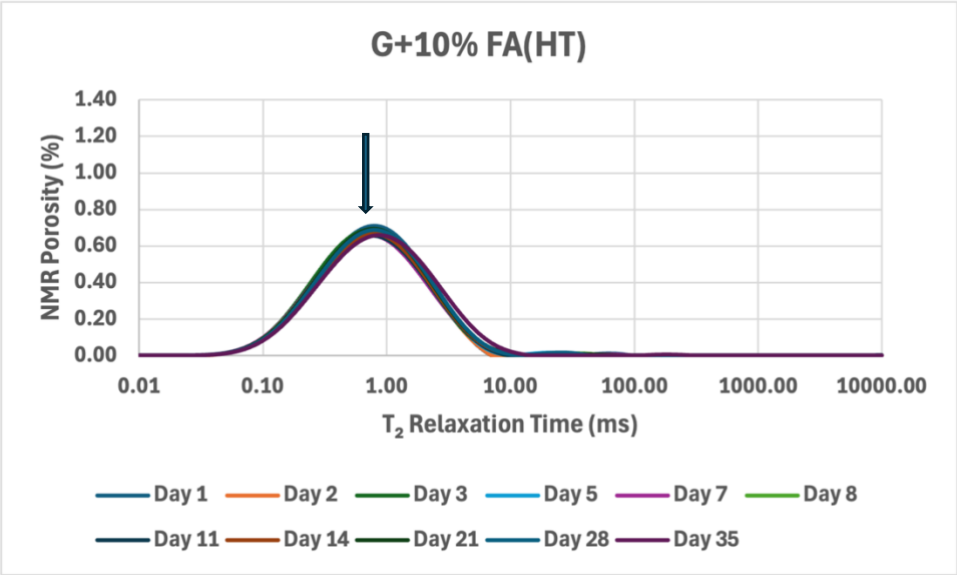

Figure 57: T_2 distribution profile for G+10% FA cured at high-temperature conditions on selected days

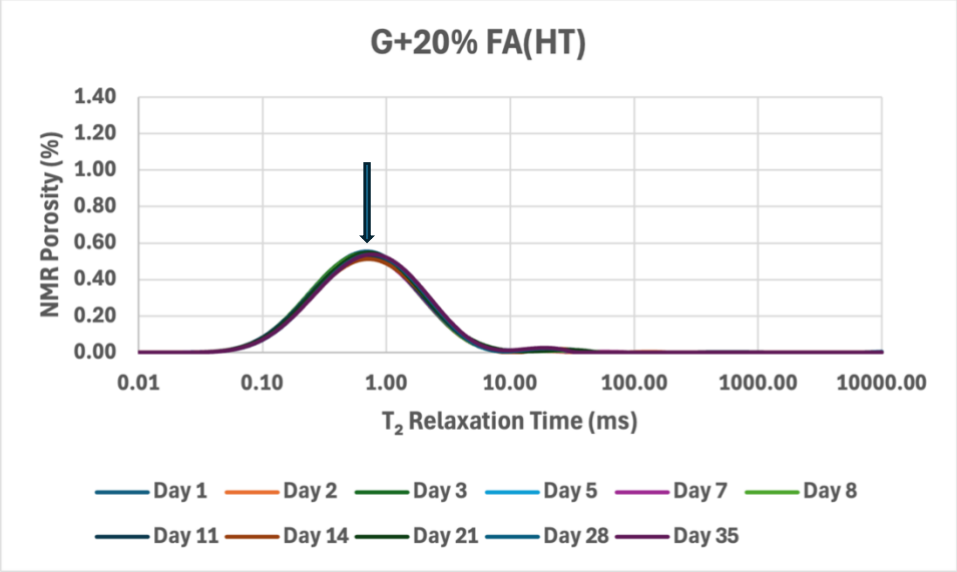

Figure 58: T_2 distribution profile for G+20% FA cured at high-temperature conditions on selected days

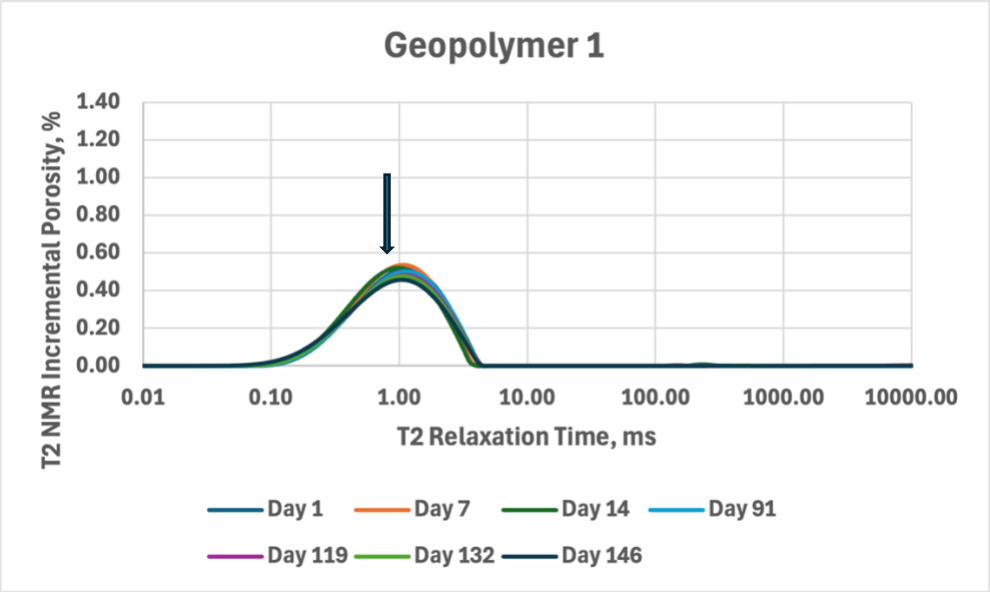

Figure 59: T_2 distribution profile for geopolymer cured at high-temperature conditions on selected days

5.8 Geopolymer and Traditional Formulations

The geopolymer sample exhibited consistently lower NMR porosity compared to traditional class G cement formulations with various additives. Starting at 8.3% and gradually declining to 7.8% by Day 146, the Geopolymer maintained a relatively stable porosity, indicating an inherently dense microstructure with minimal changes over time. In contrast, traditional cement formulations, such as Class G with 5% Microblock, 10% Silica Flour, 5% Microcellulose, or 10% Fly Ash, started with significantly higher porosity levels (ranging from 20.2% to 30.3%) and showed more substantial reductions over the 146 days. This means that while traditional formulations rely heavily on ongoing hydration and additive interactions to improve density, the geopolymer's initial low porosity and limited changes indicate a fundamentally different and more stable pore structure from the outset which could be attributed to geopolymers generally requiring less water in their

initial mix compared to traditional recipes. The lower water demand during formation means fewer voids are created as water evaporates, reducing residual pore spaces and lowering overall porosity

6 Conclusions

This research presents a detailed and systematic investigation of the long-term porosity behavior of class G, class H, and Geopolymer cement formulations used in well cementing using non-destructive testing by leveraging on Nuclear Magnetic Resonance (NMR) technology to monitor porosity changes over extended curing periods. It also focuses on the effects of various additives-fly ash, microblock, microcellulose, and silica flour on the porosity of cement. Additionally, the study specifically evaluates the impact of incorporating different percentages of fly ash by weight of cement at high temperature curing conditions on the porosity of class G cement.

- An analytical examination has established a direct correlation between the addition of additives and a consequential enhancement in NMR porosity.
- NMR analysis demonstrated that incorporating fly ash into class G and class H effectively reduced long-term NMR porosity under room temperature conditions.
- Curing time influenced NMR porosity behavior, with prolonged curing leading to further reductions in porosity. The results showed that extended curing allowed for continued hydration and pozzolanic reactions for samples with fly ash.
- As hydration progressed at room temperature, pore distribution analysis showed a shift in peak size toward smaller pores, indicating a gradual densification of the cement structure. The incorporation of additives accelerated this trend, suggesting that they effectively enhanced pore refinement.
- Elevated temperature tests over 35 days showed very distinct behavior of approximately stable porosity over time. The fly ash-containing samples varied by concentration and maintained lower NMR porosity levels which was achieved within 24 hours of curing. This

was evident from the more stable T_2 distribution profiles observed in high-temperature conditions, where peaks showed minimal shifts over time.

- The NMR porosity levels for the geopolymer samples cured under high-temperature conditions remained stable over the curing period, achieving levels within 24 hours of curing. Overall, the geopolymer samples had the lowest porosity levels across all samples considered in this study.
- The findings directly connect to practical applications in the oil and gas industry, showing how reduced NMR porosity and refined pore distribution achieved with certain additives enhance wellbore integrity by minimizing fluid migration and improving cement durability
- This work provides valuable insights into selecting cement formulations to improve wellbore integrity, considering the behavior of different additives on NMR porosity evolution and pore distribution. The findings guide the application of optimal cement designs tailored for specific environmental challenges in well cementing.
- While this study provides valuable insights into the porosity behavior of cement formulations, it is limited by the specific temperature ranges and additive concentrations tested. Further research is recommended to explore additional additives, long-term testing under cyclic temperature conditions, and the mechanical properties of cement in conjunction with NMR porosity measurements.

Bibliography

Abid, K., Gholami, R., Tiong, M., Nagaratnam, B., Sarmadivaleh, M., Mostofi, M., Bing, C. H., & Muktadir, G. (2019). A pozzolanic supplementary material to reinforce class G cement used for drilling and completion operations. *Journal of Petroleum Science and Engineering*, *177*, 79–92. https://doi.org/10.1016/j.petrol.2019.02.038

Aïtcin, P.-C., & Robert J. Flatt. (2016). *Science and Technology of Concrete Admixtures*. Elsevier.

Al-Salami, A. E. (2012). *The Effect of Fly Ash on Resistance of Hardened Cement Pastes ton Sodium Chloride Attack*.

Amani, M., Al-Jubouri, M., Khadr, S., & Sayed, A. (2017). Application of NMR Technology in the Evaluation of Properties of Petroleum Reservoirs. *16th International Conference on Geoinformatics - Theoretical and Applied Aspects*, 1–5.

American Petroleum Institute. (2010). *ANSI/API Spec 10A - Specification for Cements and Materials for Well Cementing*.

Ardanuy, M., Claramunt, J., & Toledo Filho, R. D. (2015). Cellulosic fiber reinforced cement-based composites: A review of recent research. In *Construction and Building Materials* (Vol. 79, pp. 115–128). Elsevier Ltd. https://doi.org/10.1016/j.conbuildmat.2015.01.035

Bageri, B. S., Adebayo, A. R., Al Jaberi, J., Patil, S., & Salin, R. B. (2021). Evaluating drilling fluid infiltration in porous media – Comparing NMR, gravimetric, and X-ray CT scan methods. *Journal of Petroleum Science and Engineering*, *198*. https://doi.org/10.1016/j.petrol.2020.108242

Barabanshchikov, Y., Pham, H., & Usanova, K. (2021). Influence of microfibrillated cellulose additive on strength, elastic modulus, heat release, and shrinkage of mortar and concrete. *Materials*, *14*(22). https://doi.org/10.3390/ma14226933

Barrie, P. J. (2000). *Characterization of porous media using NMR methods* (Vol. 41).

Bhatt, H. J., Prajapati Darshan P, Khalak, A. A., & Patel, M. J. (2023). Advancements in Cement Technology: A Comprehensive Review of Additives and Their Impact on Material Properties. *International Journal of Research Publication and Reviews*, *4*(12), 1105–1112. https://doi.org/10.55248/gengpi.4.1223.123404

Bois, A. P., Garnier, A., Rodot, F., Saint-Marc, J., & Aimard, N. (2012). Use of a mechanistic model to forecast cement-sheath integrity. *SPE Drilling & Completion*, *26*(2), 159–169.

Bouzoubaa, N., Zhang, M. H., & Malhotra, V. M. (2001). *Mechanical Properties and Durability of Concrete Made with High-Volume Fly Ash Blended Cements Using a Coarse Fly Ash. Cement and Concrete Research*. *31*(3), 1393–1402.

Brisard, S., Serdar, M., & Monteiro, P. J. M. (2020). Multiscale X-ray tomography of cementitious materials: A review. In *Cement and Concrete Research* (Vol. 128). Elsevier Ltd. https://doi.org/10.1016/j.cemconres.2019.105824

Broni-Bediako, E. (2016). Oil Well Cement Additives: A Review of the Common Types. *Oil & Gas Research, 02*(02).

Cheshire, M. C., Stack, A. G., William Carey, J., Anovitz, L. M., & Ilavsky, J. (2017). *Wellbore Cement Porosity Evolution in Response to Mineral Alteration During CO 2 Flooding 2*.

Chu, D. C., Kleib, J., Amar, M., & Benzerzour, M. (2021). *Determination of the degree of hydration of Portland cement using three different approaches: Scanning electron microscopy (SEM-BSE) and Thermogravimetric analysis (TGA)*. https://doi.org/10.1016/j.cscm.2021.e00754ï

Coates, G. R., Xiao, L., & Prammer, M. G. (1999). NMR Logging Principles and Applications. *Elsevier Science*.

Davidovits, J. (2008). Geopolymer Chemistry and Applications. *Institut Géopolymère*.

De Andrade, J., & Sangesland, S. (2016). Cement Sheath Failure Mechanisms: Numerical Estimates to Design for Long-Term Well Integrity. *Journal of Petroleum Science and Engineering*, *147*, 682–698. https://doi.org/10.1016/j.petrol.2016.08.032

Dodson, V. H. (1990). *Concrete Admixtures*. Van Nostrand Reinhold.

Dunn, K. J., Bergman, D. J., & LaTorraca, G. A. (Eds.). (2002). Nuclear Magnetic Resonance: Petrophysical and Logging Applications. *Elsevier: Amsterdam, The Netherlands*, *32*.

Dunn, K. J., Bergman, D. J., & Latorracca, G. A. (2002). *Nuclear Magnetic Resonance Petrophysical and Logging Applications*.

Duxson, P., Fernandez-Jimenez, A., Provis J. L., Lukey, G. C., Palomo, A., & van Deventer, J. S. (2007). Geopolymer technology: The current state of the art. *Journal of Materials Science*, *42*(9), 2917–2933.

Elkem. (2024). *Microblock, product details*. Microblock, product details (accessed 21-11-2016).

ExxonMobil Global Outlook. (2024). *Energy demand drivers*. https://corporate.exxonmobil.com/sustainability-and-reports/global-outlook/energy-demand-drivers

Filho, A. S., Parveen, S., Rana, S., Vanderlei, R., & Fangueiro, R. (2021). Micro-structure and mechanical properties of microcrystalline cellulose-sisal fiber reinforced cementitious composites developed using cetyltrimethylammonium bromide as the dispersing agent. *Cellulose*, *28*(3), 1663–1686. https://doi.org/10.1007/s10570-020-03641-5

Fink, J. (2015). Petroleum Engineer's Guide to Oil Field Chemicals and Fluids. *2nd.Elsevier*.

Goodwin, K. J., & Crook, R. J. (1992). Cement sheath stress failure. *SPE Drilling Engineering*, *7*(4), 291–296.

Green Imaging Technologies, Inc. (2016). *Hardware Setup and Calibration Manual.* .

Guo, J. C., Zhou, H. Y., Zeng, J., Wang, K. J., Lai, J., & Liu, Y. X. (2020). Advances in low-field nuclear magnetic resonance (NMR) technologies applied for characterization of pore space inside rocks: a critical review. In *Petroleum Science* (Vol. 17, Issue 5, pp. 1281–1297). China University of Petroleum Beijing. https://doi.org/10.1007/s12182-020-00488-0

Hornak, J. P. (2017). *The Basics of NMR. 11 1*. https://www.cis.rit.edu/htbooks/nmr/

Ichim, A.-C. (2017). *Experimental Determination Of Oilfield Cement Properties And Their Influence On Well Integrity A Thesis Approved For The Mewbourne SCHOOL OF PETROLEUM AND GEOLOGICAL ENGINEERING*.

International Energy Agency. (2023, October 24). *The energy world is set to change significantly by 2030, based on today's policy settings alone*. World Energy Outlook 2023. https://www.iea.org/news/the-energy-world-is-set-to-change-significantly-by-2030-based-on-today-s-policy-settings-alone

International Energy Agency. (2024). *Electricity 2024 Executive Summary*. https://www.iea.org/reports/electricity-2024/executive-summary

Investopedia. (2024, August 31). *What Percentage of the Global Economy Is the Oil and Gas Drilling Sector?* https://www.investopedia.com/ask/answers/030915/what-percentage-global-economy-comprised-oil-gas-drilling-sector.asp#:~:text=Why%20Is%20the%20Oil%20and,manufacturing%20of%20goods%20and%20services.

Jarrahi, M., Ruth, D. W., Bassuoni, M. T., & Holländer, H. M. (2019). Porosity Measurement of Low Permeable Materials Using Gas Expansion Induced Water Intrusion Porosimetry (GEIWIP). *Scientific Reports*, *9*(1). https://doi.org/10.1038/s41598-019-53441-6

Jennings, H. M., Bullard, J. W., Thomas, J. J., Andrade, J. E., Chen, J. J., & Scherer, G. W. (2008). Characterization and Modeling of Pores and Surfaces in Cement Paste: Correlations to Processing and Properties. In *Journal of Advanced Concrete Technology* (Vol. 6, Issue 1).

Kabir, I. I., Sorrell, C. C., Mada, M. R., Cholake, S. T., & Bandyopadhyay, S. (2016). General model for comparative tensile mechanical properties of composites fabricated from fly ash and virgin/recycled high-density polyethylene. *Polymer Engineering and Science*, *56*(10), 1096–1108.

Kar, K. K. (2022). *Handbook of Fly Ash*.

Keating, J., Hannant, D. J., & Hibbert, A. P. (1989). Correlation between cube strength, ultrasonic pulse velocity and volume change for oil well cement slurry. In *CEMENT and CONCRETE RESEARCH* (Vol. 19).

Kumar, S., Bera, A., & Shah, S. N. (2022). Potential applications of nanomaterials in oil and gas well cementing: Current status, challenges and prospects. In *Journal of Petroleum Science and Engineering* (Vol. 213). Elsevier B.V. https://doi.org/10.1016/j.petrol.2022.110395

Lavagna, L., & Nisticò, R. (2023). An Insight into the Chemistry of Cement—A Review. In *Applied Sciences (Switzerland)* (Vol. 13, Issue 1). MDPI. https://doi.org/10.3390/app13010203

Llorens, J., Julián, F., Gifra, E., Espinach, F. X., Soler, J., & Chamorro, M. À. (2023). An Approach to Understanding the Hydration of Cement-Based Composites Reinforced with Untreated Natural Fibers. *Sustainability (Switzerland)*, *15*(12). https://doi.org/10.3390/su15129388

Luke, K., Hall, C., Jones, T., Barnes, P., Turillas, X., & Lewis, A. (1995). New Techniques for Monitoring Cement Hydration Under Simulated Well Conditions. *SPE International Symposium on Oilfield Chemistry*.

Matsunaga, M., Yamamoto, H., & Tanaka, S. (2002). Influence of microblock on the thermal resistance of oil well cement. *Journal of Petroleum Science and Engineering*, *35*(1–2), 43–53.

Matsunaga, T., Kim, J. K., Hardcastle, S., & Rohatgi, P. K. (2002). Crystallinity and selected properties of fly ash particles. *Materials Science and Engineering*, *325*.

McDonald, P. J., Rodin, V., & Valori, A. (2010). Characterisation of intra- and inter-C-S-H gel pore water in white cement based on an analysis of NMR signal amplitudes as a function of water content. *Cement and Concrete Research*, *40*(12), 1656–1663. https://doi.org/10.1016/j.cemconres.2010.08.003

McKinsey & Company. (2024). *Global Energy Perspective 2024*. https://www.mckinsey.com/industries/energy-and-materials/our-insights/global-energy-perspective

Medina-Rodriguez, B. X., & Alvarado, V. (2021). Use of gas adsorption and inversion methods for shale pore structure characterization. In *Energies* (Vol. 14, Issue 10). MDPI AG. https://doi.org/10.3390/en14102880

Mehta, P. K. (1986). *Concrete: Structure, Properties, and Materials. 16*(5), 765–774.

Minja, F., & Lieberman, G. (2017, September 12). *The Basics of MRI: T1 vs. T2*. http://eradiology.bidmc.harvard.edu/LearningLab/central/minja.pdf

Mohammadi, Y., Ismail, Z., & Tawie, R. (2017). Effect of cellulose fibers on the mechanical properties and shrinkage of concrete. *Construction and Building Materials*, 183–188.

Muir, C. . E., & Balcom, B. . J. (2012). Pure Phase Encode Magnetic Resonance Imaging of Fluids in Porous Media. *Annual Reports on NMR Spectroscopy*, 81–113.

Muller, A. C. A., Scrivener, K. L., Gajewicz, A. M., & McDonald, P. J. (2013). Use of bench-top NMR to measure the density, composition and desorption isotherm of C-S-H in cement paste. *Microporous and Mesoporous Materials*, *178*, 99–103. https://doi.org/10.1016/j.micromeso.2013.01.032

Nelson, E. B. (1990). *Well Cementing*.

Nelson, E. B., & Guillot, D. (2006). *Well Cementing* (2nd ed.). Schlumberger.

Neville, A. M. (2011). *Properties of concrete* (5th ed.). Pearson Education Limited.

Nevřivová, L., Žižková, N., & Lédl, M. (2018). Influence of a Crystalline Additive on the Porosity of Cement Mortars. *Defect and Diffusion Forum*.

Nikoloutsopoulos, N., Sotiropoulou, A., Kakali, G., & Tsivilis, S. (2021). Physical and mechanical properties of fly ash based geopolymer concrete compared to conventional concrete. *Buildings*, *11*(5). https://doi.org/10.3390/buildings11050178

PennState Materials Research Institute. (n.d.). *Mercury Porosimetry*. Retrieved October 22, 2024, from https://www.mri.psu.edu/materials-characterization-lab/characterization-techniques/mercury-porosimetry

Pöllmann, H., Snellings, R., & Valentini, L. (n.d.). *Cement and Concrete-Past, Present, and Future*.

Poppe, A.-M., & De Schutter, G. (2005). Cement hydration in the presence of high filler contents. *Cement Concr. Res.*, *35*(12).

Powers, T. C. 1958. (1958). Structure and Physical Properties of Hardened Portland Cement Paste. *Journal of the American Ceramic Society*, *41*(1).

Provis, J. L., & Bernal, S. A. (2014). Geopolymers and related alkali-activated materials. *Annual Review of Materials Research*, *44*, 299–327.

Provis, J. L., & van Deventer, J. S. J. (2009). Geopolymers: Structure, Processing, Properties and Industrial Applications. *Woodhead Publishing*.

Puertas, F., Goñi Elizalde, S., Hernandez, M. S., Guerrero Bustos, A., Varga, C., Palacios, M., Dolado, J. S., Zhu, W., & Howind, T. (2011). *Hydration of C 3 S, C 2 S and their Blends. Micro-and Nanoscale Characterization*.

Ramachandran, V. S. (1995). *Concrete Admixtures Handbook: Properties, Science, and Technology* (2nd ed.). Noyes Publications.

Rashad, A. M. (2015). An exploratory study on high-volume fly ash concrete incorporating silica fume subjected to thermal loads. *Journal of Cleaner Production*, *87*(1), 735–744.

Romero, M., Devers, C., & Teodoriu, C. (2022). *Observations of Thermal Cracking Propagation in Geopolymer Curing*. https://pangea.stanford.edu/ERE/db/GeoConf/papers/SGW/2023/Romero.pdf

Roshan, H. (2010). *Characteristics of Oilwell Cement Slurry Using CMC*.

Safiuddin, M., & Hearn, N. (2005). Comparison of ASTM saturation techniques for measuring the permeable porosity of concrete. *Cement and Concrete Research*, *35*(5), 1008–1013. https://doi.org/10.1016/j.cemconres.2004.09.017

Saleh, F. K., Teodoriu, C., & Sondergeld, C. (2021). Review of nmr studies for oilwell cements and their importance. In *ChemEngineering* (Vol. 5, Issue 2). MDPI AG. https://doi.org/10.3390/chemengineering5020018

Šeputytė-Jucikė, J., Kligys, M., & Sinica, M. (2016). The effects of modifying additives and chemical admixtures on the properties of porous fresh and hardened cement paste. *Construction and Building Materials*, *127*, 679–691. https://doi.org/10.1016/j.conbuildmat.2016.10.014

Shafizadeh, A., Gimmi, T., Van Loon, L. R., Kaestner, A. P., Mäder, U. K., & Churakov, S. V. (2020). Time-resolved porosity changes at cement-clay interfaces derived from neutron imaging. *Cement and Concrete Research*, *127*. https://doi.org/10.1016/j.cemconres.2019.105924

Soja, W., Georget, F., Maraghechi, H., & Scrivener, K. (2020). Evolution of microstructural changes in cement paste during environmental drying. *Cement and Concrete Research*, *134*. https://doi.org/10.1016/j.cemconres.2020.106093

S&P Global. (2022). *International Well Data*. https://www.spglobal.com/commodityinsights/en/ci/products/international-well-data.html

Teodoriu, C., Clausthal, T. U., Ugwu, I., Schubert, J., & A&m, T. (2010). *Estimation of Casing-Cement-Formation Interaction using a new Analytical Model*. http://onepetro.org/SPEEURO/proceedings-pdf/10EURO/All-10EURO/SPE-131335-MS/1741736/spe-131335-ms.pdf

Thomas, M. (2007). Optimizing the Use of Fly Ash in Concrete. *Portland Cement Association*, *5420*.

Tracz, T., & Zdeb, T. (2019). Effect of hydration and carbonation progress on the porosity and permeability of cement pastes. *Materials*, *12*(1). https://doi.org/10.3390/ma12010192

United Nations. (2024). *Our Growing Population*. https://www.un.org/en/global-issues/population#:~:text=The%20world%20population%20is%20projected,surrounding%20these%20latest%20population%20projections.

Unosson, J. E., Persson, C., & Engqvist, H. (2015). An evaluation of methods to determine the porosity of calcium phosphate cements. *Journal of Biomedical Materials Research - Part B Applied Biomaterials*, *103*(1), 62–71. https://doi.org/10.1002/jbm.b.33173

U.S. Energy Information Administration. (2020, June 15). *Global electricity consumption continues to rise faster than population*. https://www.eia.gov/todayinenergy/detail.php?id=44095

U.S. Energy Information Administration. (2023, December 27). *U.S. Oil and Natural Gas Wells by Production Rate*. https://www.eia.gov/petroleum/wells/

Yakoot, M. S., Elgibaly, A. A., Ragab, A. M. S., & Mahmoud, O. (2021). Well integrity management in mature fields: a state-of-the-art review on the system structure and maturity. In *Journal of Petroleum Exploration and Production* (Vol. 11, Issue 4, pp. 1833–1853). Springer Science and Business Media B.V. https://doi.org/10.1007/s13202-021-01154-w

Ye, G., Liu, X., De Schutte, G., Poppea, A.-M., & Taerwe, L. (2007). Influence of Limestone Powder Used as Filler in SCC on Hydration and Microstructure of Cement Pastes. *Cement and Concrete Composites*, *29*(2), 94–102.

Zhang, M., & Bachu, S. (2011). Review of integrity of wellbore cement in CO_2 sequestration wells. *International Journal of Greenhouse Gas Control*, *5*(1), 40–50.

Zhu, Q., Yang, Y., Lu, X., Liu, D., Li, X., Zhang, Q., & Cai, Y. (2019). Pore structure of coals by mercury intrusion, N2 adsorption and NMR: A comparative study. *Applied Sciences (Switzerland)*, *9*(8). https://doi.org/10.3390/app9081680